



# Bioscene

**Bioscene**  
**Volume- 21 Number- 04**  
**ISSN: 1539-2422 (P) 2055-1583 (O)**  
**[www.explorebioscene.com](http://www.explorebioscene.com)**

## Comparative Studies of Cerium Oxide using Green and Chemical Synthesis on Biological and Photo Catalytic Applications as Reactive Free Radical Species: A review

Anuj Kumar<sup>1</sup>, Anita Bisht<sup>2</sup>, Ajay Singh<sup>3</sup>, Manisha<sup>4</sup>, Sarvesh Kumar<sup>5</sup>,  
Ritu Vishnoi<sup>6</sup>, Navneet Swami<sup>7</sup>, Payal Verma<sup>7</sup>, Peeush Singhal<sup>8</sup>

Corresponding Author: **Dr. Peeush Singhal**

---

**Abstract:** Cerium oxide nanoparticles (CeO<sub>2</sub> NPs) have garnered significant attention due to their unique redox properties, making them promising candidates for various biological and photocatalytic applications, particularly in mitigating reactive free radical species. This review provides a comprehensive comparison of CeO<sub>2</sub> NPs synthesized via green and chemical methods, focusing on their efficiency and effectiveness in biological and photocatalytic applications. Green synthesis, utilizing plant extracts, microorganisms, and other eco-friendly resources, is emerging as a sustainable alternative to traditional chemical synthesis. This method not only reduces environmental impact but also imparts unique properties to the nanoparticles, such as enhanced biocompatibility and reduced toxicity. On the other hand, chemical synthesis methods, while offering precise control over particle size and morphology, often involve hazardous chemicals and energy-intensive processes, which may limit their applicability in environmentally sensitive areas. The review examines the role of CeO<sub>2</sub> NPs in scavenging reactive oxygen species (ROS) and reactive nitrogen species (RNS) in biological systems, highlighting their potential in therapeutic applications such as neuroprotection, anti-inflammatory treatments, and cancer therapy. Additionally, the photocatalytic properties of CeO<sub>2</sub> NPs are analyzed, particularly in environmental remediation processes like water purification and pollutant degradation. Through a comparative analysis, the review aims to elucidate the advantages and limitations of both synthesis approaches, providing insights into their practical applications and future prospects in combating reactive free radical species. The findings suggest that while green synthesis holds promise for safer and more sustainable production of CeO<sub>2</sub> NPs, further research is needed to optimize their properties and expand their applications in both biological and environmental contexts.

**Key Words:** Cerium Oxide, Green and Chemical Synthesis, Photocatalytic Applications, reactive free radical

---

### Introduction

Metal oxide nanoparticles are the most popular and have an important role in applications in diverse fields such as medicine [1], imaging [2], energy storage [3], fuel cell, and catalyst [4] to nanomedicine. Metal oxide nanomaterials enhance the properties of bulk materials and molecules and driving force for the development of new technologies for the future. The various properties of nanomaterials are related to the increase in the surface area to volume of nanoparticles that affects the physiochemical properties that cause the new attractive applications such as UV absorption ability [5], UV emitters [6] phosphors [7][8], solid electrolytes and electrochromic devices [9], cool LEDs [10], Solid oxide fuel for a lithium-ion battery [11], supercapacitor [12], solid lubricants [13], solar cells [14]. In the last twenty years, metal oxide nanoparticles (NPs) have had potential applications in wastewater treatment as they showed higher toxicity against ordinary heterotrophic organisms, anaerobic, and ammonia-oxidizing bacteria and hence used for environmental protection [15].

Cerium (Ce) is one of the most important *n*-type semiconductor metals and high abundance naturally occurring of lanthanide series in the periodic. Cerium rare-earth metal in the Earth's crust. Cerium is malleable, soft, and ductile in nature. Cerium has its unique electronic configuration  $[\text{Xe}]-4f^1, 5d^1 6s^2$ . The energy of the inner 4f level is almost equal to the energy of the valence electron [16]. Cerium oxide materials have cubic-fluorite-type oxide with  $F_{2g}$  symmetry and oxygen vacancy [17]. Cerium oxide of nanoscale can exist in redox  $\text{Ce}^{+3}/\text{Ce}^{+4}$  sites into their 4f shell of ions and has been an important material and applied in various applications as polishing agents [18], sunscreen [19][20], panthenol stabilized cerium oxide NPs used as cosmetic purpose as to protect cells under oxidative stress by UV radiation [21], UV shielding materials [22], [23], automatic exhaust catalytic [24], [25], gas sensors [26], humidity sensors [27, 28, 29], xylene sensors [30], ZnO–CeO<sub>2</sub> nanocomposite as glucose sensor [31], selectively controlled shape ceria nanorods are effective chemical sensors [32]. The nanowire structure of ceria acts as a Gas sensor for CO gas [33]. Green synthesized cerium oxide with neem oil is used as biofuel [34].

Cerium oxide nanomaterials are also used in biotechnological applications as luminescence bio probes and contrast agents for X-ray computed tomography [35], antimicrobial therapies [36], and antibacterial and antioxidant properties [37]. Ceria is widely used as a semiconducting material because of its large band gap energy of 3.14 eV and excitation binding energy. In materials fields applications to develop luminescent materials and ionic conductors [38], optical devices [39], cerium oxide-coated carbon microspheres capable of enhancing the catalytic ozonation activity [40], and industrial applications [6]. Nickel-doped ceria used magnetic data storage devices [41], used as anti-corrosion coating materials due to the super hydrophobicity, UV-resistance, low-cost industrial applications [42], durability, and corrosion resistance [43], solid oxide fuel cell [44]. The colloidal cerium oxide nanoparticles showed anticorrosion activity on the aluminium alloy [45]. The nanoceria acts

photocatalysts to degrade Rhodamine B (RhB) dye as water pollutants [46]. Sensing properties like enzymatic mimics [47], and the food packaging industry [17]. rGO-  $\text{CeO}_2$  nanocomposite is used as an excellent photocatalyst for the dye degradation capacity. It degrades 90 % of MB dye due to the small bandgap [48]. Rosalia Cuahtecntzi-Delint et al 2012 prepared  $\text{CeO}_2$  nanoparticles using surfactants to enhance the antibacterial activity twenty times against *E. coli* [49].

The nanomaterials can be divided into different classes according to their dimensional namely 0D, 1D, 2D, and 3D. Highly symmetric isotropic spheres, cubes, decahedra, and tetrahedra are classified as 0D nanostructures. They have an important role in nanoscience and nanotechnology. Rods, cylinders, wires, and tubes are examples of 1D nanostructures. Discs, ribbons, and plates with polygon shapes belong to 2D nanostructures [50]. Nanocerias of different shapes like nanospheres [51], nanorods [52], and controlled synthesis of nanorods by solvothermal using ethylenediamine (40-50 nm diameter and 0.3-2  $\mu\text{m}$  in length) [39], nanowires [53], nanoneedles [54].

In recent years various methods have been developed to improve the physiochemical and biomedical properties of the nanoceria. Some of the important ones are the wet chemical method [55], hydrothermal method [56], [57] a citric acid-mediated hydrothermal method [58], homogenous precipitation method [59], [60], sonochemical method [61, 62] a mechanochemical method [63], a composite-hydroxide method [64], Oleate-mediated nanoceria of uniform-size, monodispersed with size 5-20 nm showed strong violet/blue photoluminescent emission at 400 nm [65]. Self-assembly system [66], solvent deficient synthesis [67]. The various methods of synthesis of ceria were hydroxide-mediated precipitation methods. The prepared sample has a crystalline of size 9-16 nm, face-centered cubic, fluorite structure, and nanosphere of 18-30.4 nm size with an absorption peak at 325 nm in biomedical as neurotoxicity [68]. Ammonium acetate mediated chemical precipitation, prepared to nanowires and nanoneedles [54]. Monodispersed  $\text{CeO}_2$  nanoparticles synthesized by homogenous precipitation method in an alcohol/water solvent mixture [59]. Ultrafine single crystalline (size less than 6 nm)  $\text{CeO}_2$  nanoparticles with a 100 % productivity ratio using composite hydroxide molten method [64].  $\text{CeO}_2$ -PA TFN membrane nanocomposite prepared through the polymerization method is used for water treatment [69].

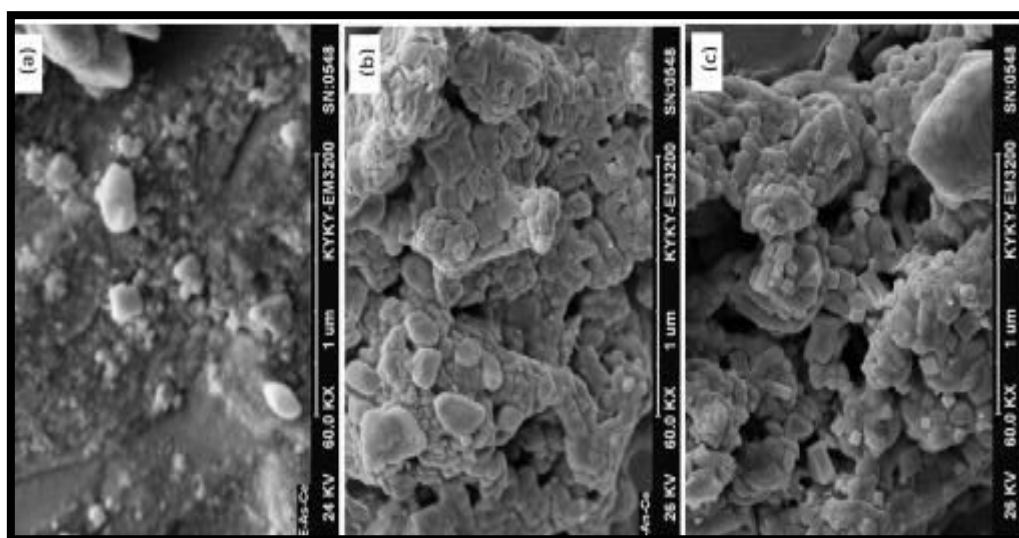
The reactive free radical species are those species that are very reactive such as oxygen, nitrogen, sulfur, and chloride. These species produce oxidative stress in the cell that results in damage to the protein, lipids, DNA, and the electron transport system of the cell. These species also have an advantage in the degradation of organic pollutants like organic dyes, and hazardous chemicals into less carcinogenic compounds. These free radical species have both beneficial and adverse activity. The beneficial activity is like the biological activity against bacterial, fungal, and viral infections. The anticancer activity and antioxidant activity were observed by the nanoceria due to the production of the free radical

species. In this review paper, we are going to discuss the comparative study of the physiochemical properties of nanocerium through chemical and green methods of synthesis. In the second part how, the physiochemical properties affected the reactive and unstable free radical species in nanocerium and showed biological and photocatalytic activity.

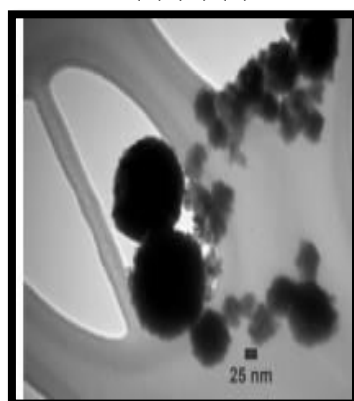
### **1. Chemical Method of Synthesis**

The development of cerium oxide nanoparticles has been accomplished chemically in a variety of ways. Some methods were to prepare nanocerium by various chemical methods like Co-precipitation, sonochemical synthesis, hydrothermal crystallization, microemulsion, microwave, thermal decomposition, spray pyrolysis, sol-gel method, solvothermal synthesis, etc.

**1.1. The wet chemical method**-The wet chemical synthesis is also known as the solution process. In this method of synthesis, various metal nanomaterials with controllable sizes, shapes, and physiochemical properties were synthesized. The functional qualities of the nanoparticles, optical, electrical, catalytic, magnetic, etc. are affected by their morphological, structural, and chemical characteristics, which were controlled during the nanomaterials formation. Au nanoparticles are loaded on the ceria nanorod surface through a wet chemical process.  $\text{NaBH}_4$  is used as a reducing agent, and the NPs have higher catalytic activity for the CO oxidation process than  $\text{CeO}_2$  NPs [70]. This method is used to prepare  $\text{CeO}_2$  NPs using  $\text{CeCl}_2 \cdot 5\text{H}_2\text{O}$  in HCl medium and ethanol in water (1:1) ratio by volume. After that two solutions are mixed dropwise with continuous stirring, to maintain the pH at 2. Then the precipitate was at  $70^\circ\text{C}$  for 4 h, calcined the product was at  $600^\circ\text{C}$  and  $1000^\circ\text{C}$  for 4 h. XRD, SEM, TEM, FTIR, and UV-vis techniques were used for characterization. The crystalline phase was cubic fluorite, with increasing temperature it changes to cubic-like with less agglomerate. TEM images showed nanospheres of 20 nm size.  $\text{CeO}_2$  nano sample observed a strong absorption peak in the UV-vis region at the 380 nm range with a direct band gap was 3.26 eV [58]. In another study, the CNP's catalytic properties were modulated with the anion of the precursor salts. The physical properties and surface chemistry were affected by the anions of the precursors during synthesis by the wet chemical method in the presence of  $\text{H}_2\text{O}_2$ . The prepared nanocerium has excellent SOD-mimetic activities and antioxidant properties [71].



(a)(b)(c)



(d)

**Figures -1-a,b,c** are SEM images of the  $\text{CeO}_2$  nanoparticles prepared by the Wet chemical method.

**Figure-1d-** is a TEM image of the  $\text{CeO}_2$  nanoparticles prepared by the Wet chemical method. Reference [58]. Copyright 2016 Hanyang University Press

**1.2.The hydrothermal method-**Hydrothermal method is one of the most effective methods for the synthesis of metals-based nanomaterials, the most cost-effective, facile, and extensively used route for the synthesis. Wei Wang et al (2010) synthesize the tunable morphologies of ceria nanomaterials of nanorods (5-10

nm), nanowires (40 diameters, length-3-10  $\mu\text{m}$ ), and nanospheres (12 nm), without using template and surfactant. In their study, they demonstrated that changing the precursor ions and their concentration affects the morphologies of the products. The precursor  $\text{Cl}^-$  ions define the nanowire while  $\text{NO}_3^-$  ions tune to the nanospheres. The replacement of the  $\text{Cl}^-$  by  $\text{PO}_4^{3-}$  ions changes the morphology and shape from nanowires to nanorods [72]. The different morphology and sizes of ceria nanoparticles were prepared by using surfactants such as CTAB, and SDS, and capping agents like PVP in the same concentration using a hydroxide mediated hydrothermal approach. The particles of size 40-100 nm were formed using SEM images [73]. Rongrong Cui et al. (2009) created a spherical  $\text{CeO}_2$  nanostructure by using trisodium citrate dihydrate as a shape controller for the fabrication of 3D-nanoflakes via a simple hydrothermal process that did not require the use of a template. The temperature and reaction time affected the size, surface morphology, and crystalline nature of the nanostructure. Because of the high surface area BET surface of  $24\text{ m}^2/\text{g}$ , the products formed at  $200^\circ\text{C}$  for 24 h act as a very good oxidative catalyst for CO combustion [74]. Abbas et al. (2016) prepared  $\text{CeO}_2$  nanostructured microspheres with homogenous multilayers of an average size of 40 nm using citric acid. The prepared sample from the hydrothermal method was a nanosheet that has the presence of oxygen vacancy than the untreated sample. The nanosheet has very good antibacterial properties due to the oxygen vacancy on the surface of the sample with the bandgap energy was 3.12 eV [75]. Shama Sehar et al. 2020 prepared two-shaped nanoceria by using the hydrothermal method. The precursor cerium nitrate with a mixture of oleic acid, tert-butylamine, and toluene was used for the synthesis. The solution is then autoclaved at two different temperatures  $180^\circ\text{C}$  and  $200^\circ\text{C}$  respectively. Then an oparticle syn the sized at  $180^\circ\text{C}$  were spherical in shape and Cubical shaped at  $200^\circ\text{C}$  [76]. Spherical-shaped nanoceria was prepared by facile and hard template-free hydrothermal method. The morphology of the prepared nanoceria was controlled by using various surfactants. Both types of nanosphere have excellent UV absorption capacity so they are used as ultraviolet shielding materials [22]. Similarly, the citric-based nanoceria of size 3.1 nm was prepared by hydrothermal method. The citric acid acts as a protective agent and inhibits the agglomeration of nanoparticles with an average size of 3.1 nm [5]. The nanoceria was prepared from the combustion method using different fuels like urea, glycine, glucose, and citric acid. The nature of fuel affects the crystalline and morphology of the sample. The sample prepared from urea is used as anticorrosion pigments while other fuels are used for the inhibitor reservoirs due to high the porosity [77]. T. Divya et al. in this study characterized that the hydrothermally prepared nanoceria showed more crystalline with cubic structure and  $\text{Ce}^{+3}$  species with high oxygen defects that enhance the oxygen storage capacity [78]. Zirconium-doped cerium oxide nanomaterials (3 % and 5 % doping of Zr) prepared by hydrothermal method. The particle size is in the 10-15 nm range with a smooth, random, non-uniform distribution of particles from the SAM



image[8].The hydrothermal preparation of (1D)CeO<sub>2</sub>NPs of different sizes, morphology, structure, and optical properties depends on the conc. of NaOH, temperature, and time of synthesis. The nanotubes of nanoceria of different ranges of 5-29, 12-36, 12-38, and 13-59 nm at different times of 6, 12, 24, 48, and 72 h of synthesis. The best conditions for the formation of nanotubes were 10M NaOH, 125 °C, 72 h, concentration, temperature, and time respectively of reaction to give the highest yield. That makes the ceria nanotubes an excellent photocatalytic properties under visible radiation[89]. Formaldehyde-assisted hydrothermal method of preparation 1D nanoceria nanorods of crystalline size of 21 -27 nm range. The nanoceria has very good humidity sensing properties as excellent reusable (11-97 %) with very fast response (5 sec) towards the humidity[29].

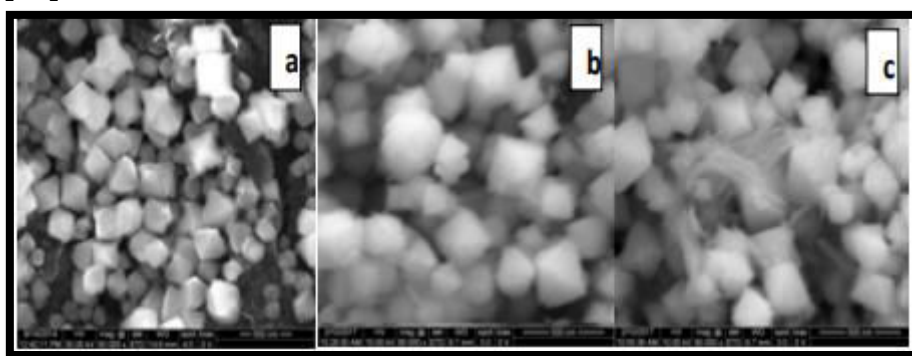


**Figure 2-** SEM images of (a) undoped CeO<sub>2</sub> (b) 2mol % Gd (c) 8mol % Gd doped CeO<sub>2</sub> nanoparticles. Prepared hydrothermally Ref[81]. Copyright 2017 Oriental Scientific Publishing Company

**1.3. Chemical precipitation methods:** Al-doped nanomaterials of ceria have been prepared by precipitation method using chloride salts of respective metals and ammonia as precursors. The sample characterization was done by XRD, SEM, TEM, and DRS. The particle formed size was 6-20 nm. The band gap of the doped nanostructures was decreased with the doping concentration of Al due to their size [82]. The nanoceria was prepared by the precipitation method using precursor materials such as cerium nitrate and ammonia and using the stream of O<sub>2</sub> and N<sub>2</sub> gas. The reaction pH, temperature, and atmosphere affect the shape and morphology of the nanoparticles. The average size of the particles was increased by increasing the temperature and decreasing the oxygen amount, and the morphology of the particle was altered from square to hexagonal. Above 50% concentration, the forms are a mix of hexagonal and needle-shaped. The band gap energy increases with the decreasing size of nanoparticles [60]. The doping of iron on cerium oxide nanomaterials affects the size of nanoparticles. The band gap energies of both direct and indirect decreases and lattice parameters increase with the increase in the concentration of iron [83]. In the presence of CTAB surfactants, the Fe-loaded nanoceria was prepared by the co-precipitation method. The TEM images showed the average



diameter of the Fe-loaded nanoceria was about 50 nm with uniform and less agglomeration [84]. Quantum-size (4-5 nm) nanoceria of spherical shape was prepared by a simple homogeneous ammonia precipitation method [85]. Recently the nanoceria were prepared by a simple and cost-effective method co-precipitation method using cationic surfactants CATB. TEM image showed the average particle size of 15.39 nm and oriented in (111) plane. The band gap of the sample was 2.47 eV which indicates the presence of oxygen defects and the presence of  $\text{Ce}^{+3}$  ion on the surface. The prepared sample dose (0.1-0.7 g/L) showed degradation of MB under UV radiation was 76 % and anticancer activity [86]. Zn-doped cerium oxide prepared through the co-precipitation method using oxalic acid as a reducing agent can be a promising nanomaterial for many optoelectronic applications such as solar cells, supercapacitors, sensors, and UV shielding devices [87].

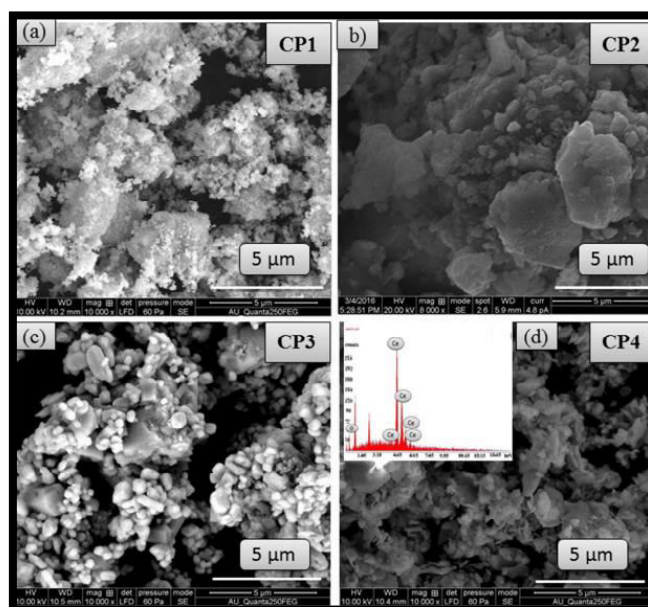


**Figure.3-**The SEM nanoparticles prepared by co-precipitation method of varying pH as a) 9(CP1), b) 10(CP2), c) 11(CP3), and d) 12 (CP4) (Inset: EDX spectra of CP4).Reference [88]. Copyright2019 Elsevier

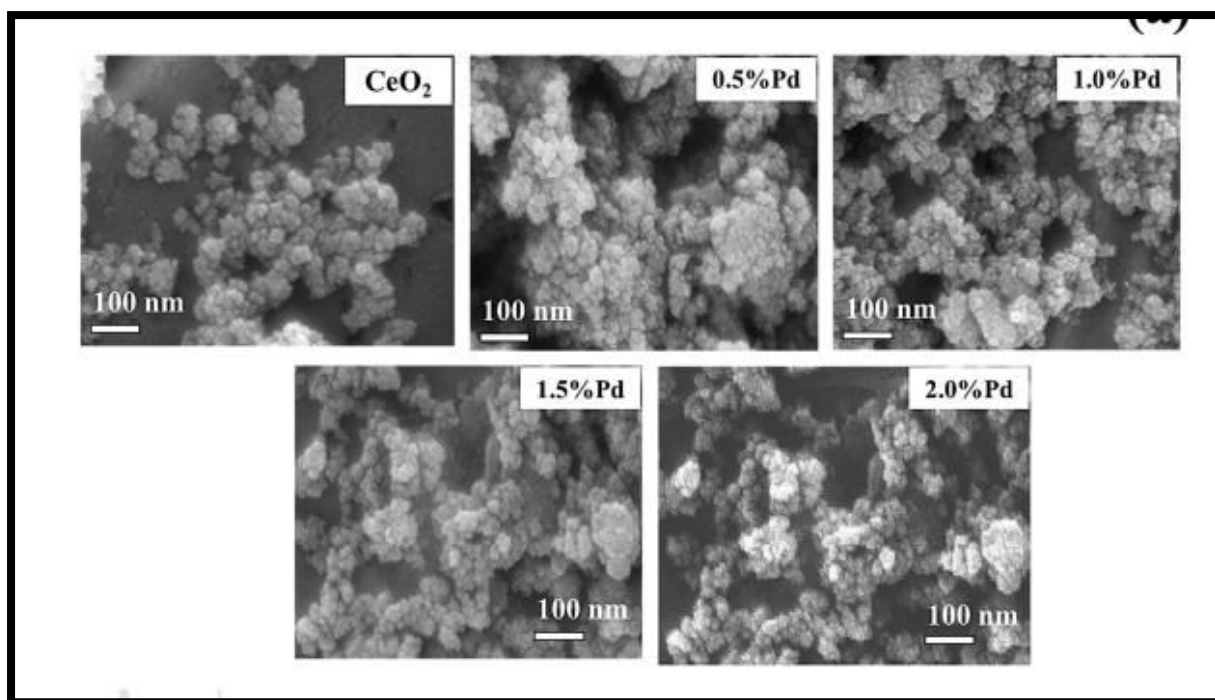


**Figure 4**-FESEM micrographs of  $\text{CeO}_2$  and different percentages of Pd-doped  $\text{CeO}_2$  nanoparticles using homogenous ppt methodRef[89]. Copyright 2018 Elsevier

**1.4. Microwave synthesis:** Siba Soren et al 2015 synthesized the nanocerium by microwave-mediated hydrothermal and microwave-mediated solvothermal methods.  $\text{CeO}_2$  nanoparticles were synthesized by polyol-mediated microwave method using different precursor salts of Cerium. The formation of nanomaterials within 10 min. XRD pattern showed the cubic crystalline and TEM, SEM images showed agglomeration and particle size was about 8-10 nm. The particles formed through the solvothermal method were less agglomerated with smaller sizes between 5 to 10 nm [90]. Similarly, the use of NaOH at 12 pH was maintained at 50 °C for 30 minutes heating a microwave. Annealing the product at 800°C for h. The spherical-shaped nanoparticles of size were around 20 nm with some agglomeration observed from SEM and TEM images. The bandgap was 3.22 eV which is larger than the bulk phase due to the quantum confinement and the UV-vis absorption spectra showed a strong peak at 321 nm was in good agreement according to the size of the nanoparticles [91]

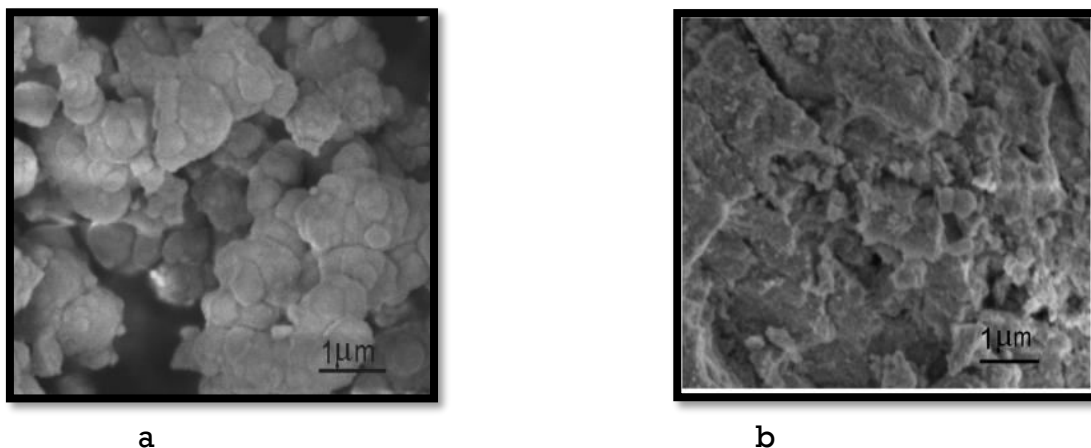


**Fig-5a)** Scanning electron micrograph image of  $\text{CeO}_2$  synthesized from  $(\text{NH}_4)_2\text{Ce}(\text{NO}_3)_6$ .

**Fig5-b)** Scanning electron micrograph image of  $\text{CeO}_2$  synthesized from  $\text{Ce}(\text{NO}_3)_3 \cdot 6\text{H}_2\text{O}$

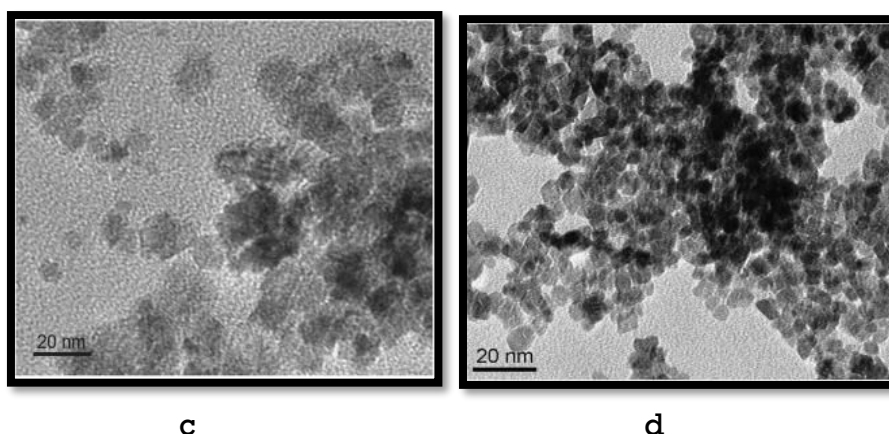


**Fig.5-c)** Transmission electron micrograph image of  $\text{CeO}_2$  synthesized from  $(\text{NH}_4)_2\text{Ce}(\text{NO}_3)_6$ .

**Fig.5-(d)** Transmission electron micrograph image of  $\text{CeO}_2$  synthesized from  $\text{Ce}(\text{NO}_3)_3 \cdot 6\text{H}_2\text{O}$ .

Ref [90]. Copyright 2015 Elsevier

**2.Green Methods of Synthesis:** Green synthesis is derived as the formation of nanostructured by using plant parts extract or microbial like algae, fungus, etc. The methods are highly safe, economical, and environmentally friendly as they don't produce any harmful by-products. S. Parvathy and B.R. Venkatraman (2017) synthesized the transition metals doped nano ceria from leaf extract of *Azadirachta Indica*. The structure, surface morphology, and elemental composition were determined by the XRD, SEM, TEM, and EDAX techniques [92]. This study proved that the mycogenesis synthesis of cerium oxide

nanoparticles have a cubic fluorite structure that is spherical at 5 nm in size and exhibits antibacterial and larvicidal activity against pathogenic bacteria and dengue vectors [93]. Spherical-shaped multifunctional nanoparticles of  $\text{CeO}_2$  were developed by using *Leucas aspera* leaf extract. The prepared nanoparticles of cubic fluorite structure with slightly higher lattice constant than the bulk counterparts because of increased oxygen vacancies.  $\text{CeO}_2$  NPs showed superior properties of photocatalytic activity against RhB dye and antibacterial activity against *E. coli* and *S. aureus* bacteria with the zone of inhibition was 4.67 and 3.33 mm respectively. These properties are mainly due to the small crystallite size, presence of oxygen vacancy surface defects, and decrease in band gap [10]. The nanocerium were prepared using the green method followed by the sol-gel method with *Rheum turkestanicum* extract as stabilizing and capping agents. The band gap decreases with the increasing the increased temperature of the annealing [94]. The green synthesized  $\text{CeO}_2$  NPs using natural materials like turmeric extract, chestnut, blossom, and pine honey with cerium nitrate salt. The prepared samples showed antibacterial, antioxidant, and photocatalytic activity. The band gap energies of the prepared samples were 2.8-3.21 eV. The average particle sizes were 1.23, 2.61, 2.61 and 3.0 nm, and spherical in shape [95]. Another study showed that the  $\text{CeO}_2$  NPs prepared through the green synthesis route of synthesis using *Dillenia indica* extract showed remarkable antioxidant properties through the DPPH assay. Therefore, prepared samples of nanocerium act as pharmacological agents against various diseases caused by oxidative stress [96]. The *C. proceras* flower aqueous extract is used for the synthesis of nanocerium of size 21 nm. The prepared sample exhibits 98.64 % of photocatalytic dye degradation of methyl orange. And also showed antibacterial activity against both types of bacterial strains but higher against the Gram-negative than the Gram-positive bacterial strains [97]. In another method, a polysaccharide biopolymer alginate was used to prepare the nanocerium. The sample crystallite size of 4.6 nm with spherical uniform size was calculated from the Scherrer equation from the XRD pattern [98]. Green synthesis of nanocerium using the orange peel alcoholic extract and cerium nitrate salt. XRD confirmed the cubic nanostructure with the 20-25 nm crystallite size and average diameter of 23 nm by DLS techniques. The synthesized nanocerium have excellent anticancer activity against HeLa cancerous cells. The cell viability in the cancerous cell was lessened to about 92-93 % in different concentrations such as 10, 25, 50, 75, 100, and 125  $\mu\text{g/ml}$  of sample. The anticancer activity was mainly due to the generation of free radicals' species of oxygen like superoxide anion and hydroxyl radical. These species oxidize the macromolecules like DNA, lipids, proteins, and cell necrosis. They also showed the antioxidant properties as the results in the formation of free radical species by using the DPPH method.  $\text{CeO}_2$  NPs also showed the photodegradation of MB dye in 30-minute exposure to sunlight. This photocatalytic activity towards the MB was mainly due to the production of holes, hydroxyl, and superoxide radicals [99]. In a similar study, the nanocerium was



prepared using the *Curcuma longa* (turmeric rhizomes) extract and cerium nitrate hexahydrate after calcinated at 600 °C for 2 hrs. XRD determined the crystallite size to be 13 nm and FESEM confirmed the spherical shape with the size of nanoparticles around 70 nm. The cell viability of cerium oxide nanoparticles did not affect the BEAS-2B cells with the concentrations of the sample ranging from 5-50 µg/well. They were nontoxic to the healthy cells. [100]. The CeO<sub>2</sub> NPs showed a potential heterogeneous photocatalyst that degraded the methylene blue and methyl orange using *Matricaria recutita* extract. The antimicrobial activity (0.15-5 mg of nanoceria) increases with the increase in particle size which is mainly due to the association of reactive free radicals with oxygen species by an increase in the surface area and increased oxygen vacancies [101].

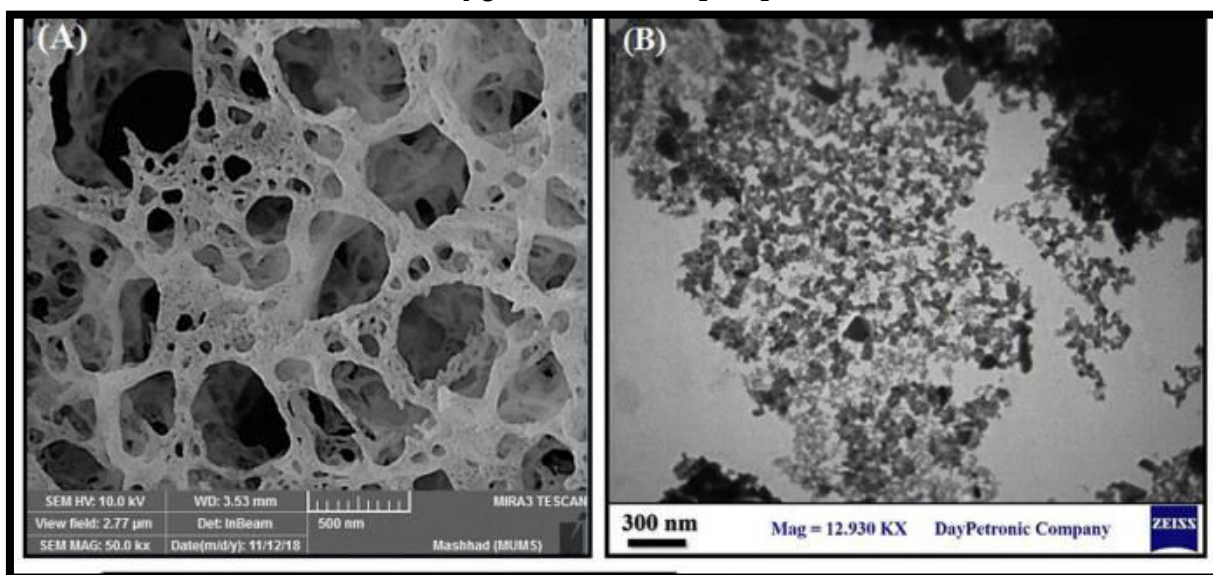


**Fig-6-A)** FESEM image and, **6-B)** TEM image, as synthesized CeO<sub>2</sub>-NPs using extract of *M. sapientum* fruit peel at 400 °C. Reference [102]. Copyright 2018 Springer

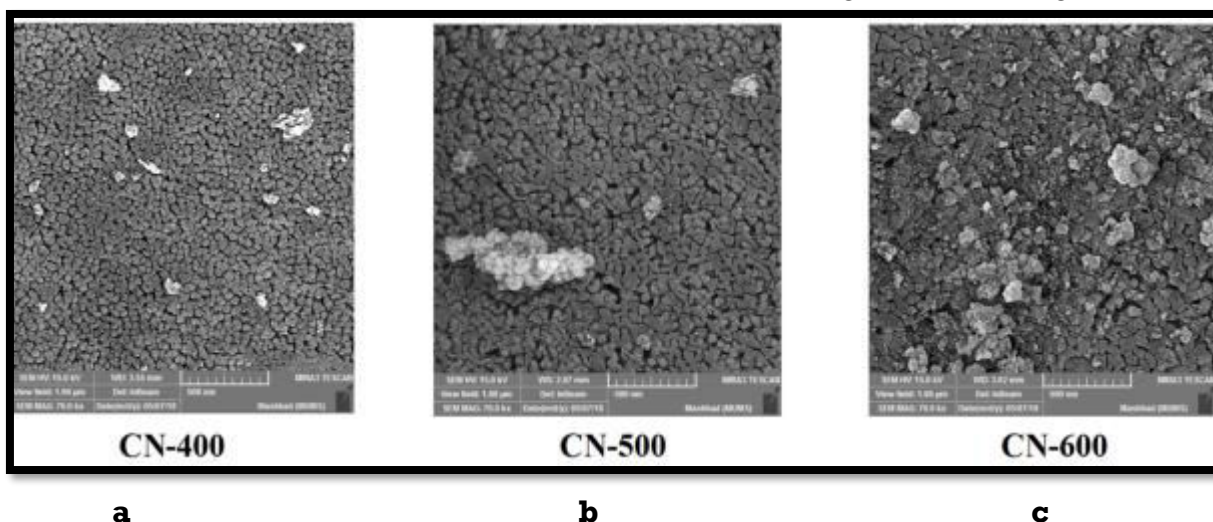


**Figure- 7a,** shows the SEM images of the size of the CN-400 particle is smaller with a more uniform morphology, **Fig.7b)** and c) showed the SEM images of CN-500 and CN-600 increasing the calcination temperature resulted in the particle

agglomeration via green synthesis by using *Cydonia oblonga miller* (Com) seeds extract Ref[103 ].Copyright 2014 Elsevier

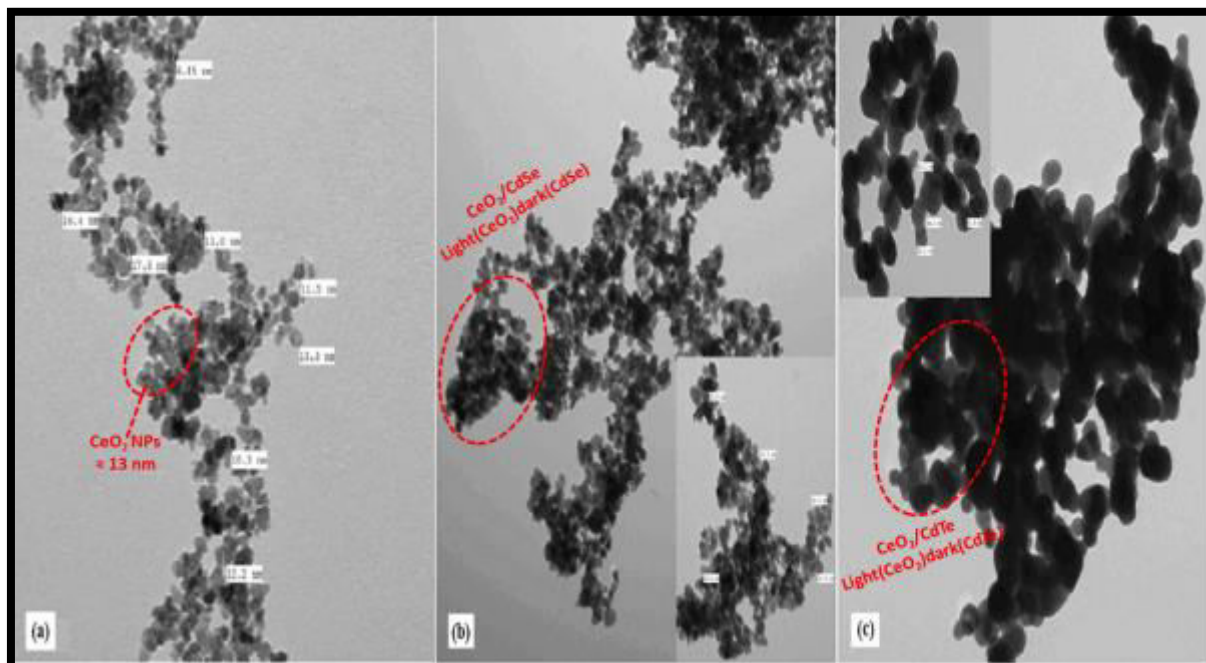
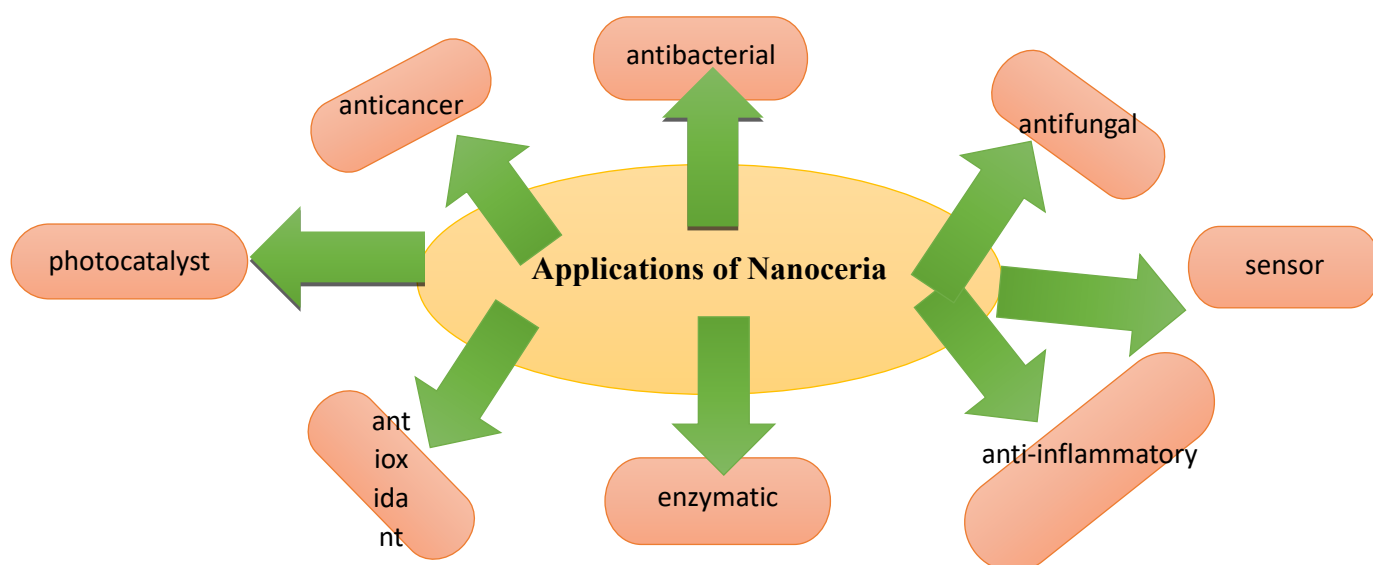


**Fig.8**-TEM images of (a) bare-CeO<sub>2</sub> NPs (b) CeO<sub>2</sub>/CdSe nanocomposite (c) CeO<sub>2</sub>/CdTe nanocomposite Reference [104]. Copyright 2021 Elsevier

**3.Applications:** Cerium oxide nanomaterials are very important in diverse fields like biological, catalyst, and various other fields. The various properties are mainly derived from the ability of the nanocerium to possess two oxidation states and their conversion from the Ce<sup>+4</sup> state to the Ce<sup>+3</sup> state. And the presence of oxygen defects in the lattice structure [105].





**3.1. Photocatalytic Activity:** The photocatalytic activity was a series of reactions carried out by the photocatalyst and remained unchanged at the end of the process. In the photocatalytic reaction, the catalyst has a small energy band gap. The photocatalytic process occurs in the absorbed phase. Semiconductors were mainly the oxides and sulfides of metals irradiated with photons, whose energy is equal to or higher than the band gap energy. The absorbed photon created the electron-hole pair, which dissociated into free photoelectrons in the conduction band and photo-holes in the valence band. The  $\text{OH}^\bullet$ , and  $\text{O}_2^\bullet$  highly reactive free radicals were generated by these holes and free electrons by the water and  $\text{O}_2$  species respectively. These reactive oxygen species then degraded the dye molecules into smaller molecules which are non-hazardous forms. The possible mechanism was proposed for the photocatalytic degradation process as: [106].

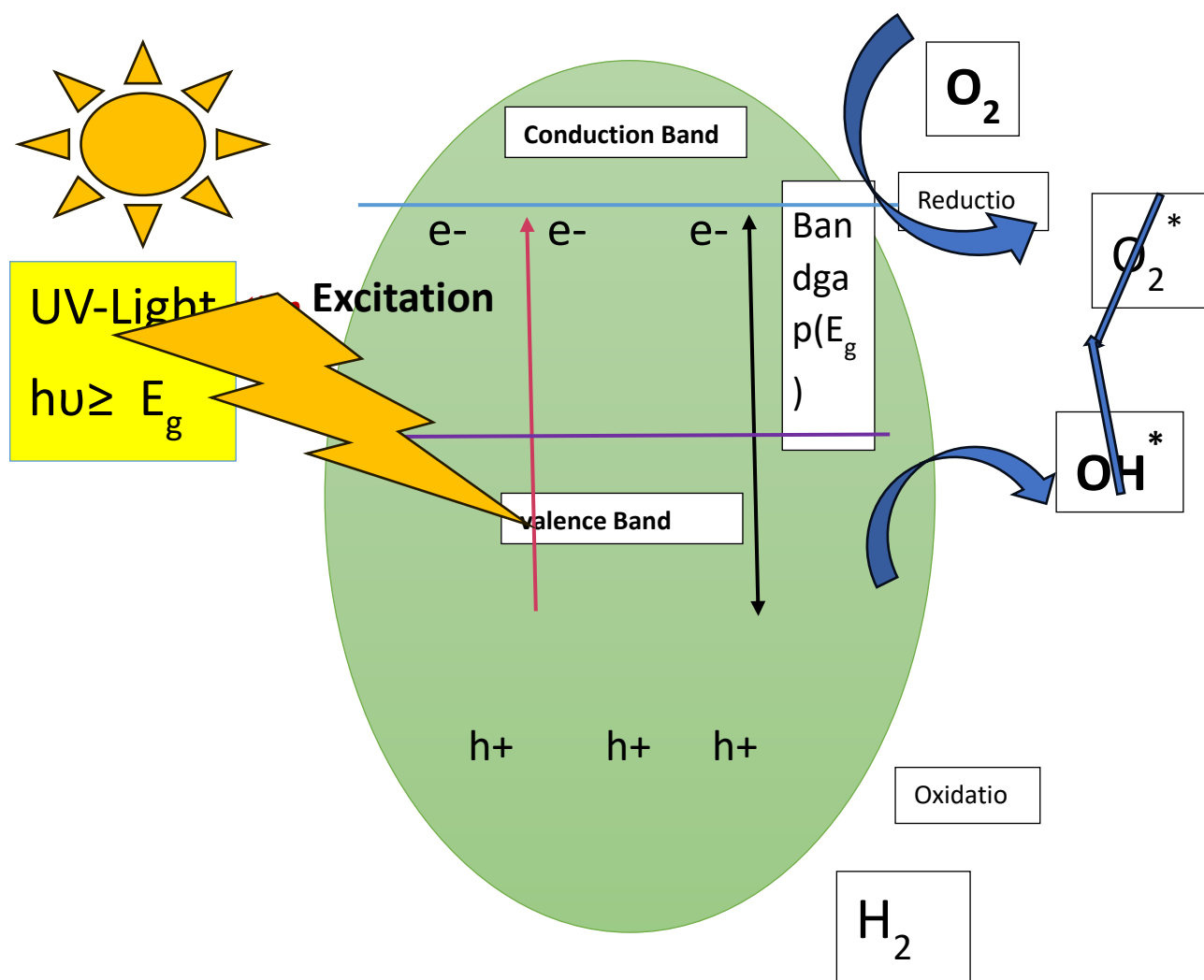
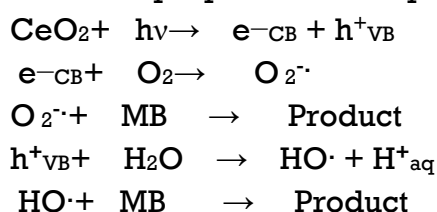
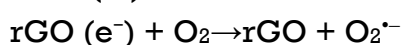
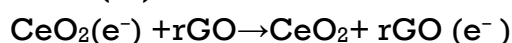
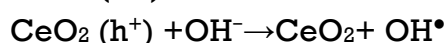
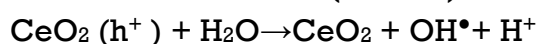
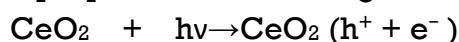


**Fig.9-Diagrammatic Presentation of the Photocatalytic Activity of nanoceria against the dye degradation by the free radical species.** Reproduction of Ref.[106]. Copyright 2022 Elsevier.

The various other parameters including crystallite size, morphology, phase composition, surface area, and structure also affect the phenomenon.

The surface of the CeO<sub>2</sub> QD of 1-10 nm size is affected by the fabrication in the structure of nanomaterials by surfactants-assisted cerium oxide NPs. The surfactants decrease the size of the nanomaterials about to the range of QD that is. 1-10 nm. The prepared QD acted as a catalyst for degrading MB at about 99.16 % under sunlight. The easy conversion of soluble Ce<sup>+4</sup> to Ce<sup>+3</sup> that easily oxidized the Fenton reagents to produce OH<sup>•</sup>. Which is a more reactive species than the peroxide to react with the MB species [107]. In another study biosynthesized CeO<sub>2</sub>-NPs of size (21 nm) were prepared using *C. procera* flower, and showed photocatalytic activity against MO to degraded MO dye about 98.64 % of 50 min under the sunlight (457 nm -λ) [108]. Similarly, the spherical-shaped nanoceria of size (4-13 nm) prepared by using banana peel showed 81.7 % photodegradation of AO7 dye in 120 min under visible light [102].

The presence of free radicals and the surface area of the nanostructured has a great impact on the catalytic activity. Recently nanoceria was prepared through the green method using *Cydonia oblonga miller* seeds. The photocatalytic degradation of Rhodamine B dye under UV-A light was approximately 94 %. The excellent photocatalytic capacity of prepared materials is because of the high surface oxygen vacancies. The surface vacant oxygen sites can take the conducting electron and decrease the recombination of electron-hole pairs. The hole reacts fast with dye molecules and degrades them [103]. Sachin Kumar et al proposed the following reaction steps for photocatalytic degradation [48].

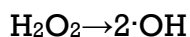
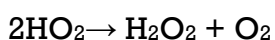
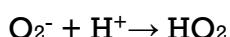
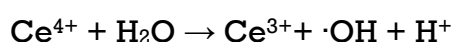
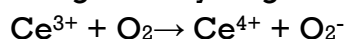


A nanocomposite of magnetic multi-walled carbon nanotube cerium dioxide is created hydrothermally. CeO<sub>2</sub> photocatalytic properties have been enhanced for methylene blue (MB) degradation (97.5%). The MMWCNTs-CeO<sub>2</sub> system is employed in the treatment of organic contaminants in wastewater [109]. Graphene oxide coated (5 wt %) -CeO<sub>2</sub> nanocomposite has a great influence on MB degradation under visible radiation. Graphene-oxide not only decreases the nanoceria particle size but also enhances the separation of the photogenerated electron-hole pair. The possible mechanism is that in irradiation under visible light the electron is transferred from the valency band to the conduction

band. The electron on the conduction band of CeO<sub>2</sub> easily migrated to the surface of the GO in the nanocomposite. The electron accumulated on the GO surface interacts with the O<sub>2</sub> molecules to produce the O<sub>2</sub><sup>-</sup>, which causes the partial decomposition of MB. The hole in the VB is directly involved in MB degradation and decreases the recombination rate of the electron-hole pair to enhance the photocatalytic activity of the catalyst [110].

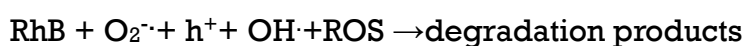
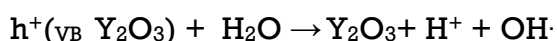
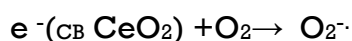
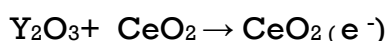
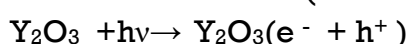
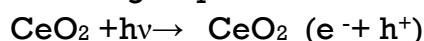
Green method using D(+)-glucose the cerium oxide-carbon microspheres were developed using the hydrothermal method. The hybrid microspheres were 5 μm in size and were an excellent catalyst in salicylic acid degradation using ozone [40]. The Pd-doping on CeO<sub>2</sub> showed the potential generation of the new energy level in the band structure of CeO<sub>2</sub>. The decreasing band gap from 3.0 eV to 2.8 eV by the presence of Pd<sup>+2</sup>. The trapping of electrons by the sub-band states of Pd<sup>+2</sup>/Pd<sup>+3</sup> and Pd<sup>+</sup>/Pd<sup>+2</sup>. The properties of the trapping decrease the electron-hole recombination process resulting in improving the Pd-doped CeO<sub>2</sub> photocatalyst performance. And increased 5 times methyl orange dye degradation than CeO<sub>2</sub> photocatalyst [89]. A similar study of Ag/CeO<sub>2</sub> nanostructured using tartaric acid as a fuel in a simple solution combustion reaction. The synthesized Ag-CeO<sub>2</sub> materials were porous in nature of ~5–7 nm average pore size. The prepared products were an excellent photocatalyst to degrade 100% Rh B dye in 150 min [111]. V<sub>2</sub>O<sub>5</sub>-CeO<sub>2</sub> nanocomposites showed a remarkable photodegradation of MB dye above 98 % in just 25 min. The V<sub>2</sub>O<sub>5</sub>-CeO<sub>2</sub>, in the presence of scavenger agent H<sub>2</sub>O<sub>2</sub>, photodegrades the MB [112].

The morphology and the BET also affect the catalytic activity. The nanoparticles of CeO<sub>2</sub> were prepared using CTAB (surfactant) by co-precipitation process. The nanorods and spherical nanoparticles are developed with an average crystalline size of 5.0–4.4 nm. The proposed mechanism for the catalytic degradation of Congo Red dye is given below [113]:



Another study has shown that cerium oxide nanoparticles are irregularly shaped and showed some agglomeration to form large-size particles (0.5–2.0 μm) due to the rapid increase in the temperature. TEM images confirmed the almost spherical with an average diameter of 15 nm which is higher than the XRD (12.2 nm). The band gap and surface area are 2.85 eV and 47.7 m<sup>2</sup>g<sup>-1</sup>. The cubic phase CeO<sub>2</sub> has the presence of +3/+4 in the sample. Due to the cubic phase and the presence of +3/+4 in the sample with a high band gap of about 2.85 eV, photosensitized by the light absorption to form a (e<sup>-</sup>/h<sup>+</sup>) pair. That generation of electrons in the conduction and hole in the valency band both leads to the formation of reactive species of oxygen and hydroxyl radicals leading to the formation of degrading

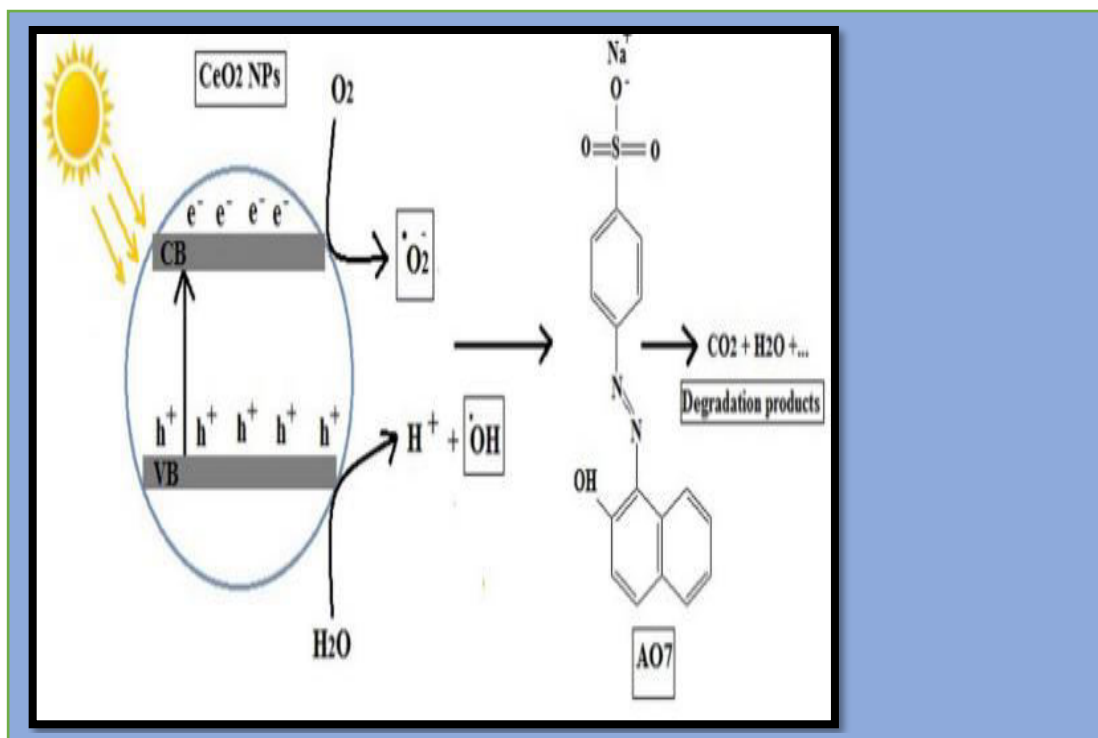
dye molecules[114]. Alia Raees et al 2021 in their study used co-precipitation to create a nanocomposite of CeO<sub>2</sub>/CuO. The average particle size was between 20-30 nm. Under visible light, they demonstrated excellent photocatalytic activity for methylene blue. The mechanism of methylene blue degradation is dependent on electron-hole separation. The visible light radiation energy was determined by the band gap between the valency band and the conduction band, which resulted in the excitation of valency electrons from the valency band to the conduction band, which created a hole in the VB and energized electrons in the CB. The production of free radicals serves as a platform for dye degradation. The synthesized nanomaterials demonstrated a very fast and efficient dye degradation catalyst towards methylene blue (MB), with times of 150 minutes and 85.66%, respectively. Due to particle aggregation on a heterogeneous surface, particles of size 25-30 nm were formed from SEM data[115]. Arthira Krishnan et al (2021) modified the catalytic properties of the nanocomposite CeO<sub>2</sub>-Fe<sub>2</sub>O<sub>3</sub> by Sn doping. The electronegativity and the ionic radii of the Ce<sup>+4</sup> were similar to that of Sn<sup>+4</sup>, during the formation of the nanocomposite the Ce ions were replaced by the Sn. That affects the size of the nanocomposite from 20 nm to 12 nm. No regular surface morphology of the nanocomposite was observed. The composite average grain size is 40 nm. This study showed that the concentration of the dopant ion affects the efficiency of the photodegradation of the catalyst[116]. CeO<sub>2</sub>-Y<sub>2</sub>O<sub>3</sub> nanocomposite photodegrades the rhodamine-B 98 % using catalyst/H<sub>2</sub>O<sub>2</sub> at 9 pH almost at 150 min. The synergic effects between CeO<sub>2</sub>-Y<sub>2</sub>O<sub>3</sub> have an important role in enhancing the photocatalytic activity of the catalyst. The possible following steps in the mechanism of nanocatalyst are given below:[117]



N. Sabari Arul 2012 study showed that the Co-doped nanocerium were prepared using the co-precipitation method without surfactants. The sample was characterized using XRD confirming the decrease in the lattice parameter due to Co doping. The morphology of the sample suggested by FESEM, and HRTEM images showed the aggregation of the nanoparticles to form the nanorods of 100-300 nm length and 10 nm diameter. The surface morphology confirmed the porous structure. The BET

surface area increases by about  $131 \text{ m}^2/\text{g}$  more than the undoped samples. The results showed 100 % photodegradation of AO7 with 10 h exposure [118]. In another study Co-doped nanoceria prepared by co-precipitation method using ethanol as solvent, homogeneous size distribution of 5-12 nm nanoparticles were formed. The doping of Co increases the oxygen defects and the band gap in the  $\text{CeO}_2$  NPs. The photocatalytic degradation efficiency of MB increases up to 98.7 % [119]. The surface defects at the catalyst surface also have important factors that affect the photodegradation efficiency. The photocatalytic degradation of organic dye methylene blue (MB) under dark, sunlight, and UV radiation. In dark the dye degradation efficiency was much lesser than in the other two conditions. The cubical nanoceria showed a 70 % efficiency than the spherical-shaped nanoceria which have about 50 %. The C- $\text{CeO}_2$  has better degradation capacity over the S- $\text{CeO}_2$  due to the high content of surface defects that enable to capture of electron-hole-pair easily and less amount of energy required as the small band gap of about  $2.82 \text{ eV}$  in C- $\text{CeO}_2$  than the S- $\text{CeO}_2$  that induced the photocatalytic reactions. It also observed that the concentration of the nanoparticles affected the degradation efficiency of S- $\text{CeO}_2$ . The increase in the concentration above  $1.0 \text{ g/L}$  (maximum degradation rate is 72 %), which causes the agglomeration in the S- $\text{CeO}_2$  particles to form clusters hence the decrease in the charge separation than the recombination ratio, shows the lower efficiency of the nanoparticles. The concentration of the dyes also affects the efficiency of dye degradation from 83.5% to 54 % when concentration was increased from 10 to  $30 \text{ mg/L}$  respectively [76]. The OPL-mediated nanoceria of spherical shape, crystal size 5.2 nm can remove 92.24 % phenol in 360 min under visible radiation [120]. The deep eutectic solvent-mediated synthesis of nanoceria was an excellent method to enhance the photocatalytic efficiency of the degradation of flumequine, effluents from the pharmaceutical industries. The DES-ceria have a much higher surface area ( $130.2 \text{ m}^2/\text{g}$ ), which provided the high accumulation of the FLU molecules on the active site of the catalyst [121]. The irregular architecture shape with a clear boundary and micro/meso surface particles of X- $\text{CeO}_2$  exhibit excellent properties of photodegradation of MB under UV-visible radiation up to six cycles. The photocatalyst has high stability in the generation of charge separation between CB and VB. The  $\text{O}_2^{\cdot-}$  and  $\text{OH}^{\cdot}$  generated from oxides and  $\text{OH}^{\cdot}$  radicals from  $\text{OH}^-$  ion in CB and VB respectively [122]. The presence of plenty of oxygen vacancy is also responsible for the photocatalytic degradation of dye. These oxygen vacancies in the nanoceria lattice which is the main source of adsorption of water molecules, act as the active sites for the water dissociation. The doping of Sm and Gd increases the lattice-free electrons and holes in nano  $\text{CeO}_2$  prepared through the microwave method. The doping affects the shape, size, and morphology of the nanoceria which directly affects the photocatalytic activity of the catalyst. Sm and Gd doped nanoceria 100 % photodegrade the MB in 16 and 14 hrs respectively into safe and nontoxic products [123]. The size and the surface area of the nanoparticles play an important role in the photodegradation activity [124].  $\text{CeO}_2/\text{CdSe}$  nanocomposite

showed photocatalytic activity(100 %)against Congo red dye for the wastewater treatment[104].The  $\text{CeO}_2/\text{rGO}$  showed excellent catalytic properties due to the  $2D\pi$  -conjugation system of rGO that eased to generate the electron hole and movement of electrons from the valence band to conduction and decreases recombination with a hole that enhances the photocatalytic activity[125].



(A)

(A)

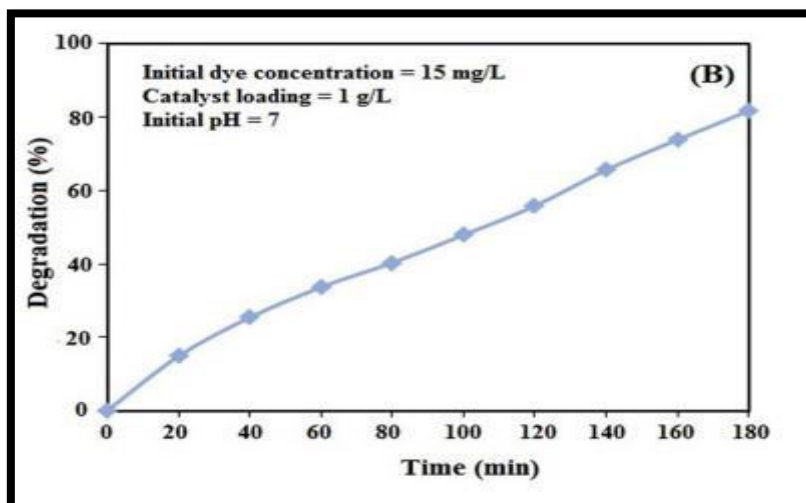




**Fig.10-(A)** Suggestion mechanism of photocatalytic activity of synthesized nanoparticles in degradation of Acid Orange 7 dye.(B) Photocatalytic degradation of AO7 under synthesized CeO<sub>2</sub>-NPs at 400 °C using biosynthesized *Musa sapientum* peel extract Ref[102]. Copyright 2021 Springer

**Table 1**–Different methods of synthesis of nanocerium using chemical and green and their Photocatalytic activity, dose of catalyst, Volume/conc. of dye solution, and removal efficiency

S. No.	Photocatalyst	Method	Size by SEM & TEM/Morphology	Pollutant	Dose of catalyst	Volume/conc. of dye solution	Removal efficiency	Time of illumination	Ref.
1	CeO <sub>2</sub>	Controlled synthesis by hydrothermal	Cubical	Methylene Blue	1.0 g/L	10 mg/L	C-CeO <sub>2</sub> -83.5 % S-CeO <sub>2</sub> -60 %	210 min	[76]
2	CeO <sub>2</sub>	Co-ppt (CTAB)	15.39 nm	Methylene Blue	0.1-0.7 g/L	10 mg/L	76 %	240 min	[86]
3	Pd - CeO <sub>2</sub>	Homogenous precipitation	10-20 nm /spherical with high agglomeration	methyl orange	0.2 g/L	20 mg/L	92 %	120 min	[89]
4	CeO <sub>2</sub>	leaves of <i>Rheum turkestanicum</i>	30 nm/spherical agglomerated and uniformed	rhodamine-B methyl orange MB	120 mg/L	1 × 10 <sup>-5</sup> M	82 % 71 % 33 %	180 min	[94]
5	CeO <sub>2</sub> -NPs	Biosynthesis from <i>Matricaria recutita</i>	12 nm	Methylene Blue & methyl orange	1 g/L	60 mg/L	93.0 %	108 min	[101]
6	CeO <sub>2</sub>	Green synthesis	4-13 nm	acid orange 7	15 mg/L	1.0 g/L	81.7 %	180 min	[102]

		by banana peel							
7	CeO <sub>2</sub> /CdS e and CeO <sub>2</sub> /CdTe	hydrothermal	20.7/20 nm	Cong Red	1 g/L	5 × 10 <sup>-5</sup> M	100 %	150 min	[104]
8	CeO <sub>2</sub>	Sonochemical method	35-38 nm spherical with porous nature	Methylene Blue	2.4 g/L	20 mg/L	90.4 %	90 min	[106]
9	CeO <sub>2</sub>	Green synthesis using <i>Calotropis procera</i> leaf extract	21 nm	methyl orange	1.0 g/L	1x10 <sup>-5</sup> M	98 .64 %	50 min	[108]
10	MMWCNTs - CeO <sub>2</sub>	Hydrothermal	-	Methylene blue	1 g/L	5x10 <sup>-5</sup> M	97.5 %	120 min	[109]
11	CeO <sub>2</sub> -graphene oxide composite	Alcohol-thermal method	-	Methylene Blue	0.1 g /L	20.0 mg /L	81 %	240 min	[110]
12	Ag- CeO <sub>2</sub>	Solution combustion method	Nanoflakes with porous nature.	Rhodamine B	1.5 g/L	2.08 x 10 <sup>-5</sup> M	100 %	150 min	[111]
13	V <sub>2</sub> O <sub>5</sub> - CeO <sub>2</sub> Nanocomposite	Precipitation-thermal decomposition	-	Methylene Blue	0.2 g/L	10 mg /L	Above 98 %		[112]
14	CeO <sub>2</sub>	green chemical precipitation method (cationic surfactant CTAB)	4.3-5.0 nm Spherical nanoparticles and nanorods	Azo dye Congo red	10 - 250 mg/L	10-100 mg/L	Nanoparticle- 90 % nanorods - 97%,	360 min	[113]

15	CeO <sub>2</sub>	Microwave mediated hydrothermal	15 nm/single cubic phase spherical	AlizerinredS Eriochrome black -T	0.8,2.0, 6.7 g/L 0.6,2.0, 6.8 g/L	100 mg/L  100 mg/L	100 %  100 %	120 min	[114]
16	CeO <sub>2</sub> /CuO Nanocomposite	Co - ppt	20-30 nm	Methylene Blue	1 g/L	10 mg/L	85.66 %	150 min	[115]
17	Sn doped (5 %)-CeO <sub>2</sub> - Fe <sub>2</sub> O <sub>3</sub> composite	Thermal decomposition	15 nm	Methyl Orange and Methylene Blue	1.0 g/L for both	10mg/L for both	94.65 % MB & 100 % MO	120 min	[116]
18	CeO <sub>2</sub> /Y <sub>2</sub> O <sub>3</sub> nanocomposite	Hydrothermal method (NaOH)	10 nm/nanopowder	Rhodamine B dye	5g/L	20 mg/L	98 %	150 min	[117]
19	Co-doped CeO <sub>2</sub>	Co-precipitation (NH <sub>4</sub> OH)	nanorods	Azodyes acid orange 7	4 g/L	0.2 M	100 %	240 min	[118]
20	Co- CeO <sub>2</sub> (doping 6 % of Co)	co-precipitation	5-12nm	Methylene Blue	1 gm/L	15 mg/L	98 %	420 min	[119]
21	CeO <sub>2</sub> -NPs	<i>Elaeisguineensis</i> leaves	13-16 nm/ uniformly agglomerated	phenol	1.0 g/L	50mg/L	92.24 %	360 min	[120]
22	CeO <sub>2</sub>	PVP - assisted hydrothermal	Length 20 µm-width 4 µm/ Micro or /mesopore	Methylene Blue	1 g/L	40 mg/L	99.9 %	120	[122]
23	Sm& Gd doped CeO <sub>2</sub>	Microwave	15-29 nm/nanorods	Methylene Blue	1g/L	1.7 × 10 <sup>-6</sup> M	99.6 %	9 hrs	[123]
24	CeO <sub>2</sub>	Solution combustion using (EDTA)	35 nm/spherical nanoparticle	Trypan blue	0.4 gm/L	5-25 mg /L	100 %	135 min	[124]

			es						
25	CeO <sub>2</sub> /rGO	hydrothermal	6.23 nm	Direct green	15g/L	20 mg/L	80 % UV	120 min	[125]
26	CeO <sub>2</sub>	<i>Elaeisguineensis</i> leaves	13-16 nm/ uniformly agglomerated particles	phenol	1.0 g/L	50 mg/L.	92.24%	360 min	[126]
27	CeO <sub>2</sub>	Marine oyster	15 nm	Methylene Blue	150 mg/L	150 mg/L	99 %	60 min	[127]
28	CeO <sub>2</sub>	Green synthesis <i>Moringa oleifera</i>	45 nm spherical	Crystal violet	5 mg/L	10 mg/L	97.5 %	60 min	[128]
29	CeO <sub>2</sub>	Green <i>Jatropha curcas</i>	18-25 nm	acetaldehyde	-		99.6 %	-	[129]
30	CeO <sub>2</sub>	Green synthesis <i>A. indica</i> leaf extracts	10-15 nm with uniform size	Rhodamine B	10g/L	10 mg/L	96 %	120 min	[130]
31	Eu doped CeO <sub>2</sub>	Glycine assist hydrothermal	15-20 nm, spherical with some agglomeration	Cong Red			67 % UV-visible	120 min	[131]
32	Er- CeO <sub>2</sub>	Hydrothermal method	20 nm and diameter 35 nm/nanorod	Rhodamine B dye	5 g/L	20 mg/L	94 %	40	[132]
33	CeO <sub>2</sub>	hydrothermal	23 nm spherical/	Methylene Blue	0.5 g/L	1mmol	-	-	[133]
34	CeO <sub>2</sub>	Precipitation	Nanorods, 82.3 nm	methyl orange	5g/L	1.5 x10 <sup>-4</sup> M	50 % UV	80 min	[134]
35	CeO <sub>2</sub>	Solution combustion using watermel	Agglomeration with irregular morpholog	Methylene blue	10 mg/L	10 mg/L	98 %	180 min	[135]

		on juice	y						
--	--	----------	---	--	--	--	--	--	--

**3.2. Biological Activity:** The cerium oxide nanoparticles showed potential applications in the biological fields. They showed anticancer, antioxidant, anti-inflammatory, and antimicrobial activity. The biological properties of nanoceria are mainly due to the existence of two oxidant states,  $Ce^{+3}$  and  $Ce^{+4}$ . The interchanging of these two states can form an oxygen vacancy on the surface of the nanoceria. The band gap energy of the nanoceria is responsible for creating holes and the reactive free radical species. Both these factors are responsible for the biological activity in nanoceria.

### 3.2.1. Antibacterial activity

The antibacterial activity of the nanomaterials was counted regarding the various parameters. These parameters like size, surface morphology, surface area, the charge on particles, and the reaction medium. The antibacterial mechanism occurs mainly two-step process. In step first, the nanomaterials are adsorbed on the surface of the bacterial membrane. Since the bacterial membrane is negatively charged on the surface, that causes the interaction between the cell wall and the nanomaterials. The second step after the adsorbed onto the bacterial membrane causes oxidative stress and interferes with the internal nutrients of the cell [136].

Green synthesis of cerium oxide nanoparticles using *Prosopis juliflora* leaf extract ultrasound-assisted method evaluated the antibacterial activity against both Gram-positive (G+) bacteria and Gram-negative (G-) bacteria. The disc diffusion assay was performed by a zone of inhibition test with around CONPs MICs, about 0.1 ml. In *P. aeruginosa*, *P. vulgaris*, showed mild to moderate activity while the case of *S. aureus* and *S. pneumonia* showed the highest antibacterial activity due to their different cell membrane and cell wall composition [36]. Ag/CeO<sub>2</sub> composite (12-31 nm) has an average porous nature (5-7 nm). They exhibit excellent antibacterial activity against both gram-positive and gram-negative bacterial strains. The minimum inhibition concentration of the Ag/CeO<sub>2</sub> sample was observed at 3.125 µg/ml and 6.25 µg/ml. The possible antibacterial mechanism for cell death by nanostructures is due to the production of ROS on the surface of the cell wall, which damages the bacteria's cell wall, causing cytoplasm leakage and ultimately cell death [111]. The antibacterial activity was tested using a disc diffusion test against the Gram-positive organisms and Gram-negative organisms. The antimicrobial activity was 100% against Gram-negative organisms than the others [73]. Abbas et al 2016 prepared citric acid-based nanostructures of ceria by giving hydrothermal and aging treatment. The crystalline size of 9 nm was calculated by XRD. The SEM images revealed multilayer nanosheets to form microspheres. The average size was about 40 nm as compared to nano spherical particles were 30 nm in size. The agar disc diffusion test demonstrated that the nanosheets have higher antibacterial activity than the nanospheres. The presence of oxygen vacancy over the surface enhances the interaction with the cell wall and

generates the ROS that causes ultimately cell death [75]. LU Xiao-wang et al 2012 prepared Ag/CeO<sub>2</sub> mesoporous with pore size in samples 5-7 nm. The doping concentration affects the pore size and BET surface areas. The 5% Ag/CeO<sub>2</sub> mesopores observed the complete retardation of bacterial growth by using the agar dish method against gram-negative bacterial strain. The bacterial activity was mainly due to the Ag ion on the mesopores of the sample that was produced combined with the cell membrane. The accumulation of ions on the surface of bacteria that rupture the cell membrane and intracellular fluid leakage brings cell death [137]. In the recent study shape-controlled synthesis of CeO<sub>2</sub> NPs showed antibacterial activity of C-CeO<sub>2</sub> and S-CeO<sub>2</sub> was examined against different bacterial strains using the disc-diffusion method with the standard drug oxytetracycline. The C-CeO<sub>2</sub> NPs effectively act on all bacterial strains as compared to the S-CeO<sub>2</sub> due to their cubical shape, surface-to-volume ratios, and exposed crystal facets that present a high amount of oxygen vacancies [76]. The surfactants-based (SDS, CTAB, PVP) ceria nanoparticles were synthesized using the hydroxide mediate method. The different surfactants affect the surface and morphology of the developed nanomaterials. The grain size was found to be in the 37.5-43.5 nm range with spherical-shaped morphology of the nanoparticles. The antibacterial activity was observed at 100% in gram-negative bacterial strains *Proteus vulgaris* than in the gram-positive strains *Corynebacterium diphtheria* and *Sarcina lutea*. The size and shape of nanomaterials influence the antibacterial action as the interaction with the cell wall of the bacteria or as the concentration increases leads to the internalization of the nanoparticles and causes the toxicity of the bacterial cell [138]. The dopant nanoceria inhibits bacterial growth due to their smaller size and large surface area. The cell walls of both the gram-positive and gram-negative bacteria are negatively charged. The interaction between the cell wall and the positively charged nanoparticles changes the action of the electron transport chain in bacteria. Recent studies proved that ROS generation is deeply associated with the dopant that modified the structure of nanoparticles. Green facile synthesis of Ag-doped ceria nanoparticles using saliva seeds enhanced the antibacterial activity against both bacterial strains [139]. The samarium (Sm) doped cerium oxide (size 43-58 nm) had excellent antibacterial activity due to the Sm<sup>+3</sup> doped metal as the presence of reactive oxygen species produced the oxidative stress that causes bacterial cell death [140]. Another study reported that Gd-doped CeO<sub>2</sub> nanoparticles of size 57.4-58.3 nm in cube and square shape showed excellent antibacterial activity. The main reason was the smaller-sized particles easily entered into the cell wall which causes bacterial cell death [81]. The green synthesized nanoceria by using *Acalypha indica* leaf has been reported to inhibit bacterial activity by more than 90 %. The mechanism for the antibacterial activity was that the cellular proteins became inactive as the nanoceria generated the hydrogen peroxide that causes cell death [141]. Engineered cerium oxide nanoparticles were produced through the hydrothermal method with modified



surfactants and templates free showed antibacterial activity [142]. The Co-doped nanoceria was prepared by the hydrothermal method. The face-centered cubic with crystallite of 17-20 nm in size. The doping concentration of Co decreases the size of crystallite which affects the antibacterial activity. The doping concentration was increased the antibacterial activity increased against the four pathogenic bacteria. The antibacterial mechanism may be due to the interaction between the bacterial cell wall and the nanoparticles. The smaller the size higher the interaction between them and the nanoparticles penetrate the cell and ROS is generated that causes cell death [143]. Transition metal ions doped nanoceria prepared through the green method showed excellent antibacterial activity as compared to the pure CeO<sub>2</sub> in both bacterial strains. The possible mechanism through which it acts on the microbial is by the direct interaction with the microbial cells or to produce the secondary products that cause cell death [92]. Mohammad Altaf et al. reported the green synthesized nanoceria from *Acorus calamus* extract antibiofilm activity against both gram-positive and gram-negative bacterial strains. The prepared nanoparticles successfully inhibition of biofilm of *E. coli*, *P. aeruginosa*, and *S. aureus* in all concentrations. The possible mechanism was the inhibition of exopolysaccharides (EPS) by the CeO<sub>2</sub>-NPs which is responsible for the biofilm production in the bacteria and the production of ROS [144]. Biosynthesized cerium oxide NPs from *Coriandrum sativum* leaf extract showed excellent antibacterial activity against *P. aeruginosa* and *K. pneumonia* (gram-negative strain) as compared to *Bacillus cereus*, *Bacillus subtilis* (gram-positive) [145].

**Table 2**– For the Antibacterial activity of nanoceria using chemical and green methods of synthesis, the size of nanoparticles, morphology, and concentration of nanoceria dose.

S. No	NPs	Dopant	Size in nm	Morphology	Method	Concentration of dose	Types of Bacterial strain	Zone of inhibition (mm)	Ref.
1	CeO <sub>2</sub>	-	-	Spherical	Green synthesis <i>Leucas aspera</i> (LA) leaf extract	50-100 µg/L	<i>E. coli</i> <i>S. aureus</i>	4.67 3.33	[10]
2	CeO <sub>2</sub>	Gd	58.3-57.4 <sup>D</sup>	Cubic and square shape of	Hydrothermal	1 mg/ml	<i>E. coli</i> <i>B. cereus</i> <i>S. aureus</i>	28 26 23	[81]

				uniform size			<i>S. typhi</i>	26	
3	Ce O <sub>2</sub> NPs	Transiti on metal ion doped	9-16 <sup>D</sup>	Cubic- spherical	green synthesis	-	<i>K. pneumonia</i> <i>S. aureus</i> <i>S. dysenteriae</i> <i>E. coli</i> <i>P. aeruginosa</i> <i>S. pneumonia</i> <i>P. vulgaris</i>	Active Active Active Active Active Active	[92]
4	Ce O <sub>2</sub>	-	14.95 <sup>D</sup> 5-20 <sup>T</sup>	Cubic and spherical	<i>Aspergillus niger</i>	10 mg/mL	<i>Streptococcus pneumonia</i> <i>Bacillus subtilis</i> <i>Proteus vulgaris</i> <i>Escherichia coli</i>	10.67 10.33 8.33 6.33	[93]
5	Ce O <sub>2</sub>	-	35 <sup>D</sup> 42 <sup>T</sup>	cubic	Solution combustion	500- 1000 µg/L	<i>P. aeruginosa</i> <i>S. aureus</i>	4.5 Not seen	[124 ]
6	Ce O <sub>2</sub>	-	45 <sup>D</sup>	aggregate spherical	Microwave- assisted using <i>M. oleifera</i> peel	25 µL	<i>E. coli</i> <i>S. aureus</i>	7 5	[128 ]
7	Ce O <sub>2</sub>	Eu	15-20 <sup>D</sup>	Spherical with agglomerat ion	<i>Glycine assisted</i> <i>Hydrothermal</i>	-	<i>E. coli</i> <i>S. aureus</i>	4.2 2.2	[131 ]
8	Ce O <sub>2</sub>		36 <sup>D</sup>	Agglomerat ion with an irregular porous	Solution combustion using watermelon	1000- 500 µg/L	<i>Klebsiella aerogenes</i> <i>S. aureus</i>	1.00 1.67	[135 ]
9	Ce O <sub>2</sub>	-	40-100 <sup>S</sup>	cubical shape	Hydroxide mediate method	20 µl 100 % conc.	<i>Proteus vulgaris</i> <i>Escherichia coli</i> <i>Corynebacterium</i>	5 3 Not seen Not seen	[138 ]

							<i>diphtheriae</i> <i>Sarcina lutea</i>		
10	Ce O <sub>2</sub>	Ag	62 <sup>D</sup>	Uniform spherical	<i>Salvia</i> seeds	15 µL	<i>S. aureus</i> P. <i>aeruginosa</i>	– –	[139 ]
11	Ce O <sub>2</sub>	Sm	58.3- 43.47 <sup>D</sup>	Octahedral	Hydrotherm al	1 mg/ml	<i>E. coli</i> <i>B. cereus</i> <i>S. aureus</i> <i>S. typhi</i>	20 22 25 24	[140 ]
12	Ce O <sub>2</sub>	Co	17-20 <sup>D</sup>	small leaves or feathers like on cubic shape	hydrotherma l	1mg/ml	<i>E.coli</i> <i>S. aureus</i> <i>B. cereus</i> <i>S. Typhi</i>	24 23 27 25	[143 ]
13	Ce O <sub>2</sub>	-	2 2.03 <sup>D</sup> 16.92 <sup>T</sup>	Spherical and pseudo- spherical	Green synthesis using <i>Acorus</i> <i>calamuse</i> extra ct	1,600 µg /ml	<i>S. aureus</i> P. <i>aeruginosa</i> <i>E.coli</i>	Active Active Active	[144 ]
14	Ce O <sub>2</sub> / Cd O	nanoco mposite	27 <sup>D</sup> 15 –40 <sup>S</sup> 25 to 5 <sup>T</sup>	spherical in shape, heterogene ous with more cavities	Precipitation and hydrotherma l method	200 µg/ml	<i>S. aureus</i> <i>S. pyogenes</i> <i>P. aeruginosa</i> <i>K.</i> <i>pneumoniae</i>	P H 12 14 20 16 30 35 8 13	[146 ]
15	Ce O <sub>2</sub>	-	5 <sup>T</sup>	Spherical with some aggregatio n	Neem and ginger extract	100 mg	<i>S. mutans</i> <i>S. aureus</i> <i>C. albicans</i> <i>Enterococcu</i> <i>s faecalis</i>	11 19 9 9	[147 ]
16	Ce O <sub>2</sub>	-	30 <sup>D</sup> 36 <sup>T</sup>	Porous surface homogenou s	Green synthesis using <i>Abelmoschu</i> <i>s esculentus</i>	30 µg/ml	<i>S. aureus</i> <i>K.</i> <i>pneumonia</i>	21 19	[148 ]
17	Ce O <sub>2</sub>	Fe	22 <sup>D</sup> 27 <sup>PSD</sup>	Nearly spherical with some irregularly shaped aggregates	Co-ppt using Xanthan gum	128 µg/ml	<i>Pseudomona</i> <i>s aeruginosa</i> , <i>Listeria</i> <i>monocytogen</i> <i>es</i>	active  active	[149 ]

18	Ce O <sub>2</sub>	-	13.56 <sup>D</sup>	Nanoparticles with slight agglomeration	<i>Coriandrum sativum</i> leaf extract	50 µl	<i>P. aeruginosa</i> <i>K. pneumonia</i> <i>Bacillus cereus</i> , <i>Bacillus subtilis</i>	12 9 5 6	[145]
----	----------------------	---	--------------------	-----------------------------------------	----------------------------------------	-------	-----------------------------------------------------------------------------------------------------	-------------------	-------

D- XRD, T-TEM, S-SEM

**3.2.2. Cytotoxicity:** The cytotoxicity of the cells was determined by the cell viability test in different assayed methods. The cytotoxicity of the cells has been determined by different parameters. The ROS (reactive oxygen species) generally causes oxidative stress in the cell as the damage to protein, DNA, and cell membrane. The mitochondrial activity also expresses cell viability. The cerium nanomaterials showed cytotoxicity in the cell viability test. The nanoparticles of cerium oxide were synthesized through the supercritical method to develop nanoparticles of different sizes. The cytotoxicity was assessed by using the MTT test using BEAS-2B cell lines of human lung epithelial cells. The cells were exposed to nanoparticles (5, 10, 20, 30, 40 µm/ml) of 30 nm size causing cell death. The increased ROS level caused a decrease in GSH. The genes that are responsible for oxidative stress were induced (40 µm/ml of 30 nm particles) including catalase, glutathione S-transferase, heme oxygenase-1, and thioredoxin reductase at exposure time 4 h. However, housekeeping genes like actin are not changed by nanoparticles. The chromatin condensation and caspase-3 activation in the cultured BEAS-2B suggested the death of cells by the apoptotic process. The cytotoxicity of ceria nanoparticles is mainly due to the absorption around the nuclear membrane after 1.5 h exposure [150]. Hydrothermally developed CeO<sub>2</sub> nanoparticles were toxic toward the prostate cancer cell lines (PC-3) revealed by MTT assay. The viability of the PC-3 cancer cells decreases to 20.19% after 72 hours of incubation with HT cerium (4+) oxide nanoparticles, which are more toxic to prostate cancer cells. In the HT method, cell viability was 88.08% higher than in the HL method for the normal mouse fibroblast cell line (L929). The nanoparticles were taken up by the cell through two processes: adhesion to the cell membrane and endocytosis by the cell. As a result, the surface charge of the particles plays an important role in the binding step [151].

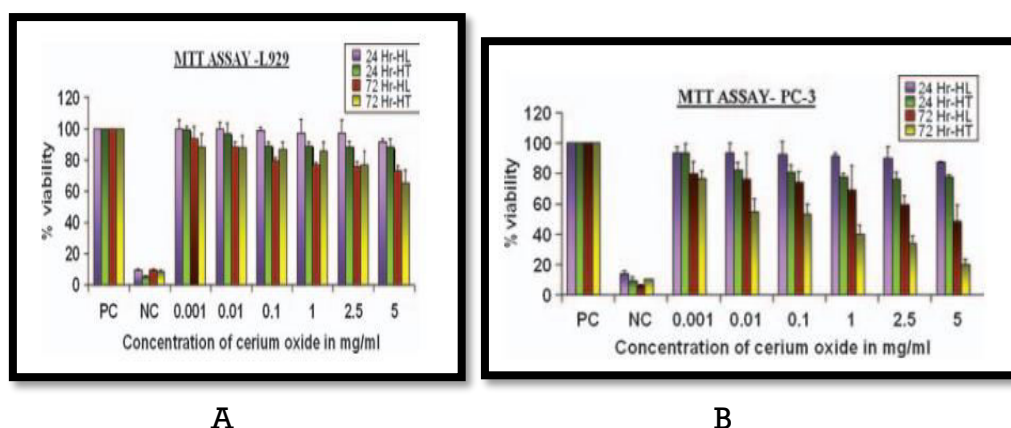


**Fig-11 A)**Hydrothermal MTT assay cytotoxicity analysis of cerium oxide nanoparticles (HT-hydrothermal, HL-hydrolysis) after 24 and 72 hr incubation in cell line L-929 and Fig-11-B) MTT assay cytotoxicity of prostate cancer cell lines (PC-3) Ref-[151]. Copyright 2016 American Scientific Publishers

CeO<sub>2</sub> NPs synthesized through the sol-gel method in a gelatin medium which acts as a stabilizer to maintain the growth of nanostructures at low temperatures. The product was a cubic fluorite structure of 10 nm in size. The in vitro cytotoxicity of CeO<sub>2</sub>-NPs was measured by the MTT method on neuro-2A cells. The cells were viable below 10 µg /mL measured by incubating for 24 h. This study set the toxicity level for future applications in different fields [173]. The particle size of nanocerium showed good optical properties that resulted in cytotoxicity. The cell viability of the PC-12 cancer cell line was detected in vitro study not affected by the nanocerium [94] and no significant toxicity was found on A549 cells prepared green method [103].

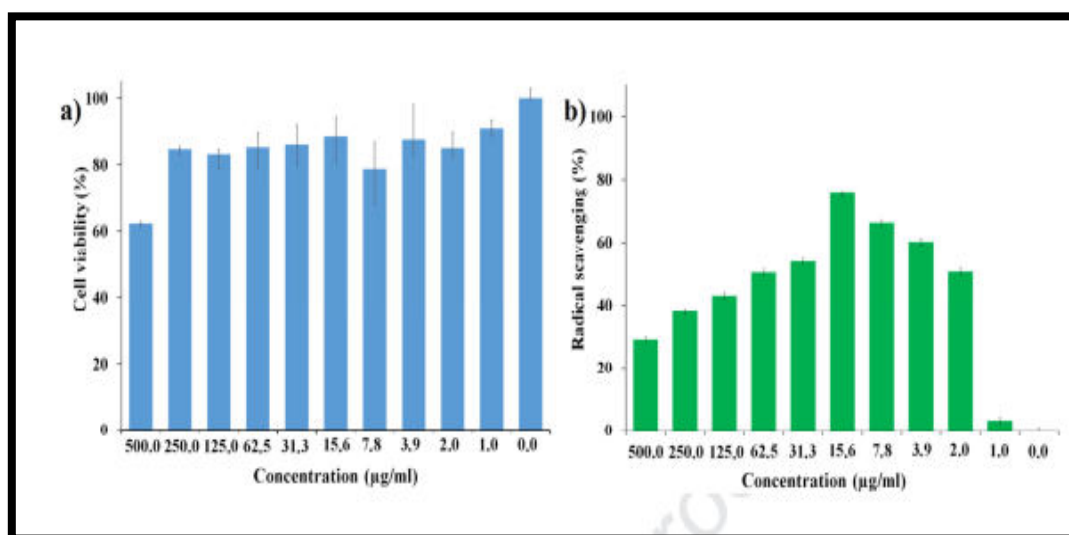


**Fig.12- a)**shows the percentage of cell viability versus various concentrations of CN-400. All concentrations of CN-400 indicated cell viability of more than 50%. **Fig. 12- b)** illustrates the percentage of ROS scavenging versus different concentrations of CN-400. 15.6 µg/ml of CN-400 had the best antioxidant influence

and could defuse about 76% of ROS formed by cellular metabolism. Reference-[103]

A study, reported by I.N. Bazhukova et al to prepare nanocerithrough the pulsed electron beam evaporation method showed cytotoxicity in four cell line dermal human fibroblasts (DHF), human embryonic kidney cells (HEK-293), human rhabdomyosarcoma (Rd), and human cervical carcinoma (HeLa) cells. The concentration of  $\text{CeO}_2$  NPs (400  $\mu\text{g}/\text{ml}$ ) does not affect the viability of healthy cell lines. However, the viability was decreased with an increase in the concentration of NPs [153]. M. Atif et al (2021) in their work showed that Mn-doped cerium oxide nanocomposite had remarkable cytotoxicity against the MCF-7 cancerous cells by reduction of the 68 % growth of cells. The doping increases the oxygen defects in the nanocerium and increases the ROS generation in the cell causing apoptosis resulting in cell death [154]. Fazal Abbas et al (2016) showed in their study that the Mn-doped cerium nanostructured sample (30-41 nm) has excellent cytotoxicity. The cytotoxicity of metal oxide depends on various parameters like particle size, electrostatic interaction between nanoparticle and cell, and the generation of reactive oxygen species (ROS). The cell viability was decreased and directly affected the ROS production. The Mn doping in  $\text{CeO}_2$  reduced the size of the nanoparticle to less than 20 nm which easily penetrated the cell and hurt the cell. In the second factor, various species of ROS were produced on the surface of the nanoparticles which increases the various process that leads the cell death like lipid peroxidation, apoptosis, and cell membrane damage. The pH level also plays an important role in measuring the cytotoxicity in  $\text{CeO}_2$ . The basic pH favours cell viability while the acidic pH enhances cytotoxicity. The 5 % Mn-doped sample inhibited the cell viability in cancer cells but not in the healthy cell line, due to the production of different levels of ROS. The ROS production is directly related to cell viability. The Mn doping also enhanced the oxygen surface defects that enhanced ROS production [155]. A similar cytotoxicity was reported by Fazal Abbas 2017 the hydrothermally prepared Sn-doped CNP (30-50 nm) size. The sample showed anticancer activity related to the generation of ROS. The anticancer activity was performed using both HEK-293 and Neuroblastoma cells. The 5 % doped sample showed that 40 % inhibited the cell viability in the cancer cell than the healthy HEK-293 cell. The nanocerium of smaller size is more effective due to band gap energies being responsible for the generation of ROS that cause cell death as the damage to their cellular DNA, mitochondria, cell membrane, and plasma protein [156]. Fazal Abbas et al reported that the increase in the Ni dopant concentration decreases the crystallite size of nanoparticles resulting in the enhancement of oxygen vacancies. That results into increase in the ROS production on the surface of the nanoparticles. The synthesized ferromagnetic nanomaterial has different cytotoxicity against the healthy cell in comparison to the cancerous cell. The cell viability decreased in the Sh-SY5Y cancer cell line up to 55 % while in healthy cells no such effect was observed [157]. In this study was observed that NPs



prepared by the three different methods: using the  $\text{NH}_4\text{OH}$  precipitation method,  $\text{NaOH}$  precipitation, and microwave hydrothermal method, have no significant cytotoxicity against neuroblastoma cells and RAW 264.7 cells [158].

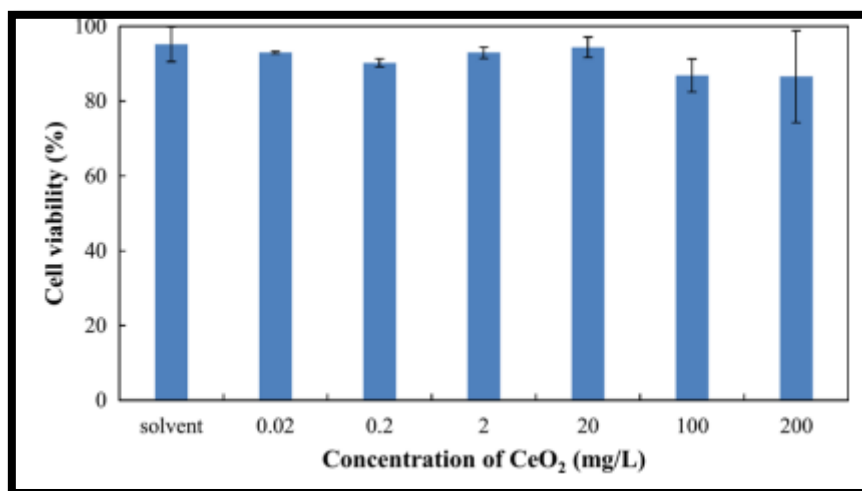


**Fig-13**-The cell viability of neuro-2a murine neuroblastoma cells by MTT assay under different concentrations of A- $\text{CeO}_2$  NP through simple  $\text{NH}_4\text{OH}$  precipitation method Ref-[158]. Copyright 2019 Springer

Abdolhossein Miri et al 2018 studied the cytotoxicity of bio-synthesized  $\text{CeO}_2$  nanoparticles that are uniform and spherical shaped with a 30 nm size observed against colon cancer cells by MTT assay. They observed the cytotoxicity of nanocerium at different concentrations (50, 100, 200, 400, 800  $\mu\text{g}/\text{ml}$ ). It was observed that no significant effect even at high concentrations of 800  $\mu\text{g}/\text{ml}$ . According to this study, the nanocerium has a potential biological application in various fields [159]. A similar study was done by Abdolhossein Miri et al 2019 that biosynthesized nanocerium using *Salvadora persica*. The synthesized  $\text{CeO}_2$  NPs Crystallite size was 19 nm from the PXRD method and morphology was uniform, almost spherical in shape from the FESEM image. The cytotoxicity was measured through an MTT assay against a colon HT-29 cancer cell line not showing toxicity (0-800  $\mu\text{g}/\text{ml}$ ) range [160].

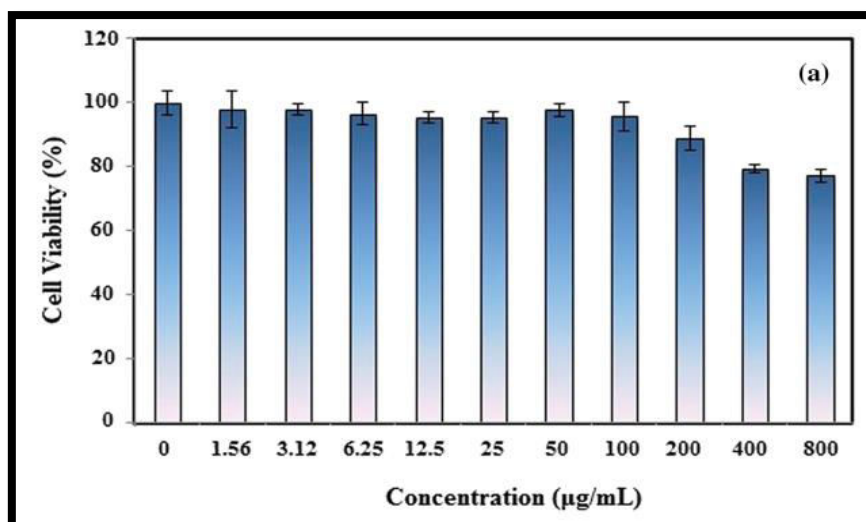


**Fig .14-** Represented the MTT cell viability assay of biosynthesized CeO<sub>2</sub>-NPs on HT-29 cancer cell lines was measured at 24 h using an aqueous extract of *Salvadora persica*. Ref [160]. Copyright 2019 Wiley

The controlled size and biosynthesis of nanoceria through green synthesis using fresh egg white followed by the different calcination temperatures (200, 400, 800 °C). The formation of nano-powder of size 25 nm, fluorite cubic structure with preferential orientation on (111) reflection plane in CeO<sub>2</sub>. The prepared nanoparticles do not have significant cytotoxicity in the periodontal fibroblast cells in all concentrations up to 800 µg/ml in vitro study [161]. Nanoceria-curcumin conjugated prepared by CeCl<sub>3</sub>·7H<sub>2</sub>O oxidation in an alkaline medium of PVP to maintain the pH at 8. Curcumin-nanoceria conjugate was prepared under vacuum conditions in various ratios of curcumin and ceria in the range of 1:1. to 1:50 molar ratio. It showed selective cytotoxicity against the human glioblastoma T98G cancer cell line than the normal cell line [162]. Esmail Nourmohammadi et al biosynthesized nanoceria through the carrageenan by sol-gel method followed by the calcination at different temperatures as 400, 500, 600, 700 and 800 °C. The surface morphology was spherical to cylindrical with little tendency for agglomeration from SEM images. The prepared NPs do not show in-vitro cytotoxicity on the WEHI-164 cell line even at high concentrations up to 250 µg/ml after 24 hrs [163]. Mohammad Ashna et al prepared cerium oxide (size of 25.46 nm) using pollen grains of *Brassica napus* and reported in-vitro toxicity against the human ovarian cancer cell. The concentration and the period affect the cell viability. The concentration of nanoceria was 12.5 µg/ml for 72 hrs which was highly lethal to the human ovarian cancer cell line while having little effect on normal human foreskin fibroblast [164]. Similar results were reported of biosynthesized nanoceria from *Ceratonia siliqua* used against the breast cancer cell line (MCF7). The toxicity increased with treatment time and concentration of nanoceria [165] and ethanolic extract *Brophyllamdaigremontianum* plant used for the preparation of nanoceria of small crystallite size and large surface area

showed excellent anticancer activity against the human breast cancer cell line MCF-7 even 50 % death of cells at lower concentration of 175.04  $\mu\text{g}/\text{ml}$  [166]. Nafas Abbasi et al reported that the Cerium oxide nanoparticles loaded on chitosan prepared using melon shell extract followed by the ion gelation method. The prepared sample was spherical with a size of 54.83 nm and had excellent cytotoxicity, decreasing the cell viability of cancer cells to 50 % and 97 % of the normal cells at the 50.65  $\mu\text{g}/\text{ml}$  concentration of the sample. The death of cells was observed mainly due to the apoptosis process [167]. A similar study done by Golnar Kermani et al revealed hybrid nano architectonics of Chitosan-Cerium Oxide Nanoparticles using rosemary leaf extract coating of chitosan around the nanoparticles by ionic gelation method. The prepared nano sample was spherical in shape with less agglomeration with 202.35 nm in size. The toxicity effect against 3 cancer cell lines AGS, A549, and PC3 in comparison with normal skin fibroblast cell lines showed. The toxicity increased on increasing the concentration of nanoparticles. The normal cells don't show toxicity at 400  $\mu\text{g}/\text{ml}$  but have high inhibitory effects on three cancer cell lines. The main mechanism of toxicity of cells was to production of pro-apoptotic genes therefore increasing expression of caspase 9 and 3 genes in the qPCR and increasing the SubG1 cell count confirm apoptosis in the cell. The ROS and oxidative damage are interrelated to cell death due to the apoptosis process [168].

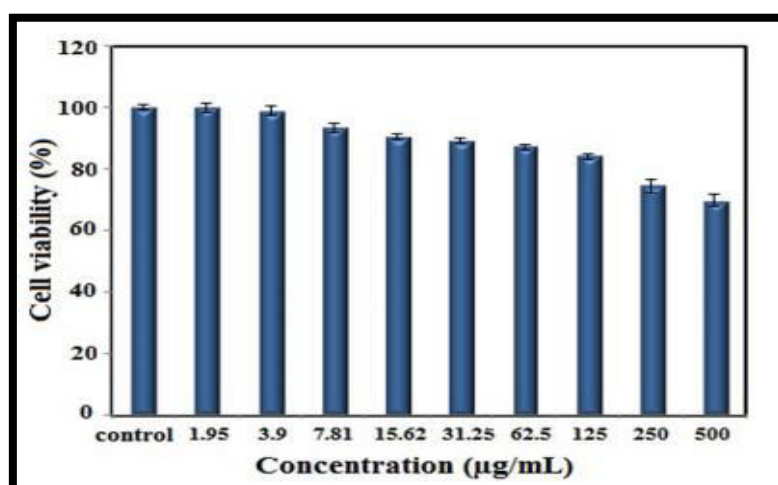


**Fig.15**-Cell viability of biosynthesized  $\text{CeO}_2$ -NPs on A549 cell line after 24 h incubation using *Musa sapientum* peel extract Ref[102] copyright 2021 Springer

**3.2.3. Neurotoxicity:** Neurotransmitter and neuromodulator, NO (nitric oxide) is required for the memory and the learning process. The generation of NO was mainly from the L-arginine by the action of some specific enzymes. However, the excessive production of the NO species combined with some ROS that are superoxide, formed peroxynitrite that was highly reactive and neurotoxic causing neuron cell death. JM Dowding 2017 in their study revealed that the nanocerium of  $\text{Ce}^{+3}$  state with fluorite structure of (3-8 nm) in size. The nanocerium

prevents the A $\beta$  or peroxynitrite production that is responsible for mitochondrial degeneration of the neuron cells. The fabricated crystalline Ag/CeO<sub>2</sub> nanomaterial has antibacterial activity against both bacterial strains. In this study, the Ag/CeO<sub>2</sub> that produces the excess amount of ROS on the surface due to the interaction with the cell wall of bacteria and nanoparticles penetrate the cell wall and kill the bacteria [111]. Neuroprotective from oxidative stress acts as an antioxidant to limit the production of reactive oxygen species that kill the cells [169].

**Table 3** –Different approaches of cytotoxicity with their methods of synthesis, effects, morphology, size, and conc. of the sample

S. N	Sample	Method of Preparation	crystallite size	Particle Morphology	Cell line	Effects	Conc. of the sample	Ref.
1	CeO <sub>2</sub>	Co-ppt (CTAB)	15.39 nm	polycrystalline nature	Human lung carcinoma cell A549	Good in-vitro anticancer activity against Human lung carcinoma cell A549 cell line	30.07 $\mu$ g/ml	[86]
2	Ag-doped CeO <sub>2</sub>	Salvia seeds extract	-	Spherical 62.7 nm	EPG 85-257 human gastric cancer cell line	No in vitro cytotoxic effects on cells up to 62.5 mM for 24 hrs after that viability of cells was decreased	62.5 mM for 24 hrs	[139]
3	CeO <sub>2</sub>	CeO <sub>2</sub> (+4) hydrothermal and CeO <sub>2</sub> (+3) hydrolysis method	HT-115 nm HL-110 nm	spherical	Human prostate cancer (PC-3) and mouse fibroblast L929	HT CNPs were viability at 88.08 % and HL CNPs at 90.9 % after 24 hrs but the +3 oxidation state did not show much toxicity to the normal cell.	5 mg/L	[151]
4	Mn-	Hydrother	105	spherical	MCF-7	Showed good in-	200 $\mu$ g/ml	

	CeO <sub>2</sub>	mal	nm		breast cancer cell line	vitro anticancer activity against the cancerous cell at 200 µg/ml concentration due to the ROS generation		[154]
5	Mn-doped CeO <sub>2</sub>	Soft chemical route	6 nm	30 -41 nm spherical in shape	Neuroblastoma cancer cell and healthy cell (HEK-293 cell)	5 % Mn-doped CeO <sub>2</sub> inhibited the viability of 40 % of cells in the cancerous cell but no cytotoxicity towards the healthy cell.	7 % Mn-doped nanoceria are toxic to both the healthy and cancerous cells.	[155]
6	Sn-CeO <sub>2</sub>	Hydrothermal	30-50 nm	20-30 nm spherical, beads like nanowires and nanosheets	Neuroblastoma cancer cell and normal HEK-293	Anticancer activity inhibition is 40 % but biocompatibility for healthy cells	20 µg/ml for 24 hrs	[156]
7	Ni-doped CeO <sub>2</sub>	Soft chemical using acetic acid as a capping agent	5 nm	22 nm, spherical homogenous particle	Sh-SY5Y cancerous and healthy human cell HEK-293	Cancer cell viability reduced up to 55 % with 7 % Ni-doped CeO <sub>2</sub> showed higher selective cytotoxicity	20 µg/ml for 24 hrs	[157]
8	CeO <sub>2</sub>	1.NH <sub>4</sub> OH precipitation 2.NaOH precipitation 3. Microwave	10.35 nm	12.87 nm spherical shape	Neuro 2A cells	No cytotoxicity effect on N2A cells	200 mg/L for 24 hrs	[158]

		hydrothermal						
9	CeO <sub>2</sub>	<i>Prosopis farcta</i> aerial part extract	Less than 30 nm	uniform with Spherical in shape	HT-29 colon cancer cells line	No cytotoxicity	800 µg/ml for 24 hrs	[159]
10	CeO <sub>2</sub>	Biosynthesis using <i>Salvadora persica</i>	19 nm	Uniform almost spherical in shape	HT-29 colon cancer cells line	No cytotoxicity	800 µg/ml for 24 hrs	[160]
11	CeO <sub>2</sub>	Fresh egg white	8-18 nm	25 nm with nanopowder of spherical shape	Human periodontal fibroblast cells	No cytotoxicity	800 µg/ml for 24 hrs	[161]
12	CeO <sub>2</sub>	Green sol-gel method		34 nm spherical and cylindrical	WEHI-164 cell line	Not seen cytotoxicity even at 250 µg/ml concentration and metabolic activity decreased maximum at 500 µg/ml conc.	250 µg/ml	[163]
13	CeO <sub>2</sub>	Pollen grains of <i>Brassica napus</i>	25.46 nm	23.2±4.0 nm with uniform and spherical	ovarian cancer cells (A2780)	Showed high toxicity effects on ovarian cancer cells (A2780) but little effect on normal human foreskin fibroblast cell line		[164]
14	CeO <sub>2</sub>	Green synthesis using <i>Ceratonia siliqua</i>	22 nm	Un-uniform, spherical shape	Breast cancer cells (MCF7)	Significantly suppress the growth of the cancer cells. The cytotoxicity	125-250 µg/ml for 48 hrs cell viability	[165]

						depends on the duration of treatment and dose		
15	CeO <sub>2</sub>	<i>Brophylla mdaigremontianum</i> plant extract	Small crystallite size	Spherical shape	Breast cancer cells (MCF7)	Cell viability decreased up to 50 % in the cancer cell line as compared to the normal L-6 cell line	175.04 µg/ml	[166]
16	CeO <sub>2</sub> NPs loaded on chitosan	Melon shell extract	5.69 nm	54.83nm, spherical to multifaceted	A549 cancer cell line and normal cell	High toxic to cancer cells and no toxicity towards normal cell	56.65 µg/ml for cancer cell and 131.108 µg/ml for normal cell	[167]
17	Hybrid chitosan - CeO <sub>2</sub>	Rosemary leaf extract	202.35 nm	mono disperse, spherical with less agglomeration	AGS, A549 and PC-3 cancer cell line	showed high cytotoxicity against all cancer cells as compared to normal cell	200 µg/ml	[168]
18	Nanoceria-curcumin conjugate	Co-evaporation with (PVP)	10-15 nm	-	Human glioblastoma T98G cell line	Showed selective cytotoxicity that caused drastic inhibition of metabolic activity and decreased the total number of tumor cells.	12.5 M	[170]
19	CeO <sub>2</sub>	Co-precipitation and Green	5-6 nm	Uniform spherical/flake	(A549) human lung cancer cell	Anticancer inhibition 40-41 %	400 µg/ml for 24 h	[171]



		synthesis						
20	CeO <sub>2</sub>	<i>Averrhoa carambola</i> leaf extract	24 nm	Micrographs of 5-10 µm, rock-like with uneven boundary and top surface net-like	Protest cancer(PC-3), colon cancer(HT-29) and breast cancer(MCF-7) cell line	CeO <sub>2</sub> NPs showed more cytotoxicity against the breast cancer(MCF-7) than Protest cancer(PC-3), colon cancer(HT-29) cell lines	20 µg/ml for 72 hrs	[172]
21	CeO <sub>2</sub>	Green synthesis	22 nm	15-20 nm	Colon cancer cell lines (HT-29)	No cytotoxic effect 400 µg/ml for 24 hrs	Cell viability 58.2 % in 500 µg/ml	[173]
22	Cd-Doped(1 & 5%) and undoped CeO <sub>2</sub>	Green synthesis using <i>Salvadora persica</i>	8.33, 11.91, 18.94 nm	15-20 nm uniform and almost spherical shape	Brest cancer (MCF-7) cell line	Cell viability was decreased by increasing the concentration of Cd to CeO <sub>2</sub> NPs. And reduced the cell viability by 50 %	-	[174]
23	Mg-doped CeO <sub>2</sub>	<i>Hibiscus sabdarifa</i>	100 nm size due to the presence of Mg	orbicular	HepG-2 (Hepatocellular carcinoma cells), MCF-7(Breast carcinoma cells), and A-549 (Lung carcinoma cells).	Biosynthesize Mg-doped acts as an excellent anticancer activity against the three cancer cell lines. The higher toxicity was observed in A-549 cells with IC <sub>50</sub> =79.19 ± 3.07 µg/mL and maximum cell inhibition of almost 96 %	109.65 ± 4.13 µg/mL (HepG2) 113.55 ± 3.89 µg/mL (MCF-7) and 79.19 ± 3.07 µg/mL	[175]
24.	CeO <sub>2</sub>	<i>Falcaria</i>	19.5	mostly	PC3 Human	Cell viability and	113.6	

	NPs	<i>Vulgaris</i> leaf extract	nm	spherical	prostate cancer cancer cells.	real-time PCR tests confirmed that the biosynthesized CeO <sub>2</sub> NPs suppress cell metastasis of the cancer cells, and enhance cell cycle arrest and apoptosis in the cancer cells.	µg/mL after 24 h treatment.	[176]
25.	CeO <sub>2</sub> NPs	Green synthesis using Carrageenan	34 nm	spherical shape	WEHI 164 cancer cell line	In-vitro cytotoxicity effects of biosynthesized CeO <sub>2</sub> NPs with the WEHI 164 cancer cell showed no cytotoxicity in the range of 0-500 and a maximum decrease in cell metabolic activity at 500 µg/ml	0-500 µg/mL after 24 h	[177]

**Antioxidant Properties:** The antioxidant species are generated by the oxidation process of the organic compounds as lipids, proteins, nuclear acids, and proteins. The ROS represents the hydroxyl OH<sup>•</sup> and O<sub>2</sub><sup>•</sup> superoxide radicals, H<sub>2</sub>O<sub>2</sub> hydrogen peroxide, and NO<sup>•</sup> radicals. These species are very reactive and cause damage to the cells and toxic effects. The presence of these ROS caused oxidative stress and induced cell death. Nitric oxide is one of the important ROS that cause the inflammatory process in the cell. The cerium NPs prepared by the solvothermal method have excellent free radicals scavenging ability. In vitro, studies showed good free radical scavenging activity for both NO and DPPH. Both nanomaterials of ceria show 55 % antioxidant activity at 75 mg ml<sup>-1</sup> concentration in the DPPH assay [178]. Another study confirms that nanocerium synthesized by simple wet chemical method nanoparticles are agglomerated with clusters of size between 5-50 nm. The prepared nanocerium

suppresses the ROS production that protects the cells. The flow cytometry test measured the nanoceria scavenging property of free radical nitric oxide in J774A.1 macrophage [179]. It has been reported that Pectin-mediated synthesized nanoceria showed a DPPH radical scavenging capacity was 73.36 % in 60 min at the 4.0 mg/mL concentration of nanoceria. Due to this property, they showed very good antibacterial activity against gram-negative bacteria than gram-positive bacteria [180]. In this study, the  $\text{CeO}_2$  was synthesized through precipitation using the mixed water-alcohol solution at constant pH = 9. The size of nanoparticles varies from 14 to 4.2 nm with the decrease in size on increasing the concentration of alcohol. The antioxidant activity was determined in two ways: i) in-vitro antioxidant activity was tested against on-cell line; ii) antioxidant property as the nano enzyme that acts as the pseudo enzyme i.e. catalase and superoxide dismutase-like behavior [181]. Green synthesized nanoceria from *Ceratonia siliqua* extract with an average size of 22 nm showed antioxidant properties. The antioxidant properties increase with the concentration of nanoparticles. The low  $\text{Ce}^{+3}/\text{Ce}^{+4}$  surface ratio affects the antioxidant catalase-mimetics activity of nanoparticles. The antioxidant properties of  $\text{CeO}_2$  NPs were investigated through the DPPH test. The prepared nanomaterials have excellent free radical scavenging capabilities than the BHA.  $\text{CeO}_2$  NPs are capable of removing DPPH radicals in a concentration-dependent by increasing the concentration of nanoparticles increasing the antioxidant property [165]. The antioxidant activity of prepared  $\text{CeO}_2$  NPs (33.31 nm) crystallite size showed a strong peak at 521  $\text{cm}^{-1}$  in Raman spectra due to the oxygen vacancy. The surface morphology shows high homogeneity with a spherical shape of average diameter 60-85.1 nm. The  $\text{CeO}_2$  NPs have excellent scavenging capabilities. The low surface ratio of  $\text{Ce}^{+3}/\text{Ce}^{+4}$  on  $\text{CeO}_2$  NPs acts as an efficient antioxidant catalytic enzyme property. The proton-donating capacity of  $\text{CeO}_2$  NPs prevents the generation of free radicals and this property increases with the concentration of the NPs [182]. Tuning the morphology of nanoceria was prepared by thermal decomposition of cerium nitrate using capping agent octylamine or oleylamine at two different temperatures. The capping agent and temperature affect nanoparticle properties like size, morphology, agglomeration, and  $\text{Ce}^{+3}/\text{Ce}^{+4}$  ratio. The antioxidant property of prepared nanoparticles was evaluated on the HaCaT human cells. The production of ROS was inhibited against the sodium arsenite (SA) induced oxidative stress [183]. Sushant et al in their study reported that  $\text{CeO}_2$  NPs can act as regenerative ROS scavengers. It acts as the SOD or catalase mimetic activity. These activities mainly depend on the surface ratio of the  $\text{Ce}^{+3}/\text{Ce}^{+4}$  valency state.  $\text{CeO}_2$  NPs showed SOD activity when  $\text{Ce}^{+3}$  (62 %) was higher than  $\text{Ce}^{+4}$  (38 %) and also on the concentration and catalase mimetic when  $\text{Ce}^{+4}$  [184]. Debanjan Dutta et al in this study resolve the contradictory behavior of nanoceria as toxic and nontoxic properties respectively. The nanoceria act as toxic when the  $\text{Ce}^{+3}/\text{Ce}^{+4}$  ratio is higher. The toxicity of NPs was mainly due to the  $\text{Ce}^{+3}$  which acts as a strong oxidizing agent. It easily donated its  $4f^1$  electron to the periphery atom

and attained the  $\text{Ce}^{+4}$  oxidation state that was more stable because of the inert gas configuration. But in the presence of oxidative stress, the  $\text{Ce}^{+3}$  higher ratio causes the antioxidant property against the ROS and appears to be highly protective in nature [185].

## Conclusion

In this review article, different methods of preparation have been discussed that have been used for the synthesis of nanoceria. The characterization and effective uses in the different fields like photocatalyst, sensor, and biomedical applications. Several chemical methods like hydrothermal, co-precipitation, microwave, wet chemical, and green methods of synthesis are very important methods to prepare nanoceria. The physicochemical properties that are directly affected by the production of ROS are responsible for the various properties in the developed Ceria NPs. Among the various chemical methods are effective but the green method approach has more advantages of synthesis as found to be eco-friendlier and more economical. This kind of synthesis approach can save time, and cost, which produces nanoceria of smaller size that are effective fields. The various factors like reaction time, pH of the reaction, different precursors, solvents, heating time, and temperature can also enhance the applications of nanoceria. The cerium oxide nanoparticles showed potential applications in the biological fields. They showed anticancer, antioxidant, anti-inflammatory, and antimicrobial activity. The biological properties of nanoceria are mainly due to the existence of two oxidant states,  $\text{Ce}^{+3}$  and  $\text{Ce}^{+4}$ . The doping affects the shape, size, and morphology of the nanoceria which directly affects the photocatalytic activity of the catalyst. The size and the surface area of the nanoparticles play an important role in the photodegradation activity. The presence of plenty of oxygen vacancy is also responsible for the photocatalytic degradation of dye. These oxygen vacancies in the nanoceria lattice which is the main source of adsorption of water molecules, act as the active sites for the water dissociation. The green synthesized nanoceria showed excellent biological activity than the chemically prepared nanoceria.

## Author Address:

<sup>1</sup>Department of Chemistry D.P.D.B.H. Govt (PG) College Kotdwar Pauri Garhwal, Uttarakhand, India

<sup>2</sup>Department of Chemistry Govt. Degree College Rudrasaprayag, Uttarakhand, India

<sup>3</sup>Department of Chemistry School of Applied and Life Sciences Uttaranchal University Dehradun, India

<sup>4</sup>Department of Botany, Chinmaya Degree College, BHEL, HARIDWAR, Uttarakhand, India

<sup>5</sup>DBS School of Pharmacy and Research, <sup>5</sup>DBS Global University, Dehradun, Uttarakhand, India

<sup>6</sup>Department of Botany, Hari Om Saraswati P.G. College, Dhanauri, Haridwar, Uttarakhand, India

<sup>7</sup>Smt. Mohari Devi Taparia Kanya Mahavidhyalaya, Jaswanthgarh, Rajasthan.

<sup>8</sup>Department of Pharmaceutical Sciences, Gurukula Kangri (Deemed to be University) Haridwar, Uttarakhand, India

## References:

- Bear, J. C., Yu, B., Blanco-Andujar, C., McNaughten, P. D., Southern, P., Mafina, M. K., ... & Parkin, I. P. (2014). A low-cost synthesis method for functionalised iron oxide nanoparticles for magnetic hyperthermia from readily available materials. *Faraday Discussions*, 175, 83-95.
- Na, H. B., Lee, J. H., An, K., Park, Y. I., Park, M., Lee, I. S., ... & Hyeon, T. (2007). Development of a T1 contrast agent for magnetic resonance imaging using MnO nanoparticles. *Angewandte Chemie*, 119(28), 5493-5497.
- Varga, E., Pusztai, P., Óvári, L., Oszkó, A., Erdőhelyi, A., Papp, C., ... & Kiss, J. (2015). Probing the interaction of Rh, Co and bimetallic Rh-Co nanoparticles with the CeO<sub>2</sub> support: Catalytic materials for alternative energy generation. *Physical Chemistry Chemical Physics*, 17(40), 27154-27166.
- Motaghi, S., & Farahmandjou, M. (2019). Structural and optoelectronic properties of Ce-Al<sub>2</sub>O<sub>3</sub> nanoparticles prepared by sol-gel precursors. *Materials Research Express*, 6(4), 045008.
- Masui, T., Hirai, H., Hamada, R., Imanaka, N., Adachi, G. Y., Sakata, T., & Mori, H. (2003). Synthesis and characterization of cerium oxide nanoparticles coated with turbostratic boron nitride. *Journal of Materials Chemistry*, 13(3), 622-627.
- Gnanam, S., & Rajendran, V. (2011). Synthesis of CeO<sub>2</sub> or  $\alpha$ -Mn<sub>2</sub>O<sub>3</sub> nanoparticles via sol-gel process and their optical properties. *Journal of sol-gel science and technology*, 58, 62-69.
- Riwotzki, K., Meyssamy, H., Kornowski, A., & Haase, M. (2000). Liquid-phase synthesis of doped nanoparticles: colloids of luminescing LaPO<sub>4</sub>: Eu and CePO<sub>4</sub>: Tb particles with a narrow particle size distribution. *The Journal of Physical Chemistry B*, 104(13), 2824-2828.
- Masalov, A., Viagin, O., Maksimchuk, P., Seminko, V., Bessalova, I., Aslanov, A., ... & Zorenko, Y. (2014). Formation of luminescent centers in CeO<sub>2</sub> nanocrystals. *Journal of luminescence*, 145, 61-64.
- Ho, C., Yu, J. C., Kwong, T., Mak, A. C., & Lai, S. (2005). Morphology-controllable synthesis of mesoporous CeO<sub>2</sub> nano-and microstructures. *Chemistry of Materials*, 17(17), 4514-4522.

- Malleshappa, J., Nagabhushana, H., Sharma, S. C., Vidya, Y. S., Anantharaju, K. S., Prashantha, S. C., ... & Surendra, B. S. (2015). *Leucas aspera* mediated multifunctional CeO<sub>2</sub> nanoparticles: structural, photoluminescent, photocatalytic and antibacterial properties. *Spectrochimica Acta Part A: Molecular and Biomolecular Spectroscopy*, 149, 452-462.
- Malleshappa, J., Nagabhushana, H., Sharma, S. C., Vidya, Y. S., Anantharaju, K. S., Prashantha, S. C., ... & Surendra, B. S. (2015). *Leucas aspera* mediated multifunctional CeO<sub>2</sub> nanoparticles: structural, photoluminescent, photocatalytic and antibacterial properties. *Spectrochimica Acta Part A: Molecular and Biomolecular Spectroscopy*, 149, 452-462.
- Maheswari, N., & Muralidharan, G. (2015). Supercapacitor behavior of cerium oxide nanoparticles in neutral aqueous electrolytes. *Energy & Fuels*, 29(12), 8246-8253.
- Sunqing, Q., Junxiu, D., & Guoxu, C. (1999). Tribological properties of CeF<sub>3</sub> nanoparticles as additives in lubricating oils. *Wear*, 230(1), 35-38.
- . Mohanty, B., Chattopadhyay, A., & Nayak, J. (2021). Band gap engineering and enhancement of electrical conductivity in hydrothermally synthesized CeO<sub>2</sub>-PbS nanocomposites for solar cell applications. *Journal of Alloys and Compounds*, 850, 156735.
- García, A., Delgado, L., Torà, J. A., Casals, E., González, E., Puentes, V., ... & Sánchez, A. (2012). Effect of cerium dioxide, titanium dioxide, silver, and gold nanoparticles on the activity of microbial communities intended in wastewater treatment. *Journal of hazardous materials*, 199, 64-72.
- Dahle, J. T., & Arai, Y. (2015). Environmental geochemistry of cerium: applications and toxicology of cerium oxide nanoparticles. *International journal of environmental research and public health*, 12(2), 1253-1278.
- Krishnamoorthy, K., Veerapandian, M., Zhang, L. H., Yun, K., & Kim, S. J. (2014). Surface chemistry of cerium oxide nanocubes: Toxicity against pathogenic bacteria and their mechanistic study. *Journal of Industrial and Engineering Chemistry*, 20(5), 3513-3517.
- Hedrick, J. B., & Sinha, S. P. (1994). Cerium-based polishing compounds: discovery to manufacture. *Journal of alloys and compounds*, 207, 377-382.
- Liu, X., Yin, S., & Sato, T. (2009, February). Synthesis and UV-shielding characterization of plate-like titanate/calcia-doped ceria composite. In *IOP Conference Series: Materials Science and Engineering* (Vol. 1, No. 1, p. 012013). IOP Publishing.
- Onoda, H., & Tanaka, R. (2019). Synthesis of cerium phosphate white pigments from cerium carbonate for cosmetics. *Journal of Materials Research and Technology*, 8(6), 5524-5528.



- Zholobak, N. M., Shcherbakov, A. B., Bogorad-Kobelska, A. S., Ivanova, O. S., Baranchikov, A. Y., Spivak, N. Y., & Ivanov, V. K. (2014). Panthenol-stabilized cerium dioxide nanoparticles for cosmeceutic formulations against ROS-induced and UV-induced damage. *Journal of Photochemistry and Photobiology B: Biology*, 130, 102-108.
- Chen, Y., Qiu, C., Chen, C., Fan, X., Xu, S., Guo, W., & Wang, Z. (2014). Facile synthesis of ceria nanospheres by Ce (OH) CO<sub>3</sub> precursors. *Materials Letters*, 122, 90-93.
- Dao, N. N., Luu, M. D., Nguyen, Q. K., & Kim, B. S. (2011). UV absorption by cerium oxide nanoparticles/epoxy composite thin films. *Advances in Natural Sciences: Nanoscience and Nanotechnology*, 2(4), 045013.
- Khan, M., Mashwani, Z. U. R., Ikram, M., Raja, N. I., Mohamed, A. H., Ren, G., & Omar, A. A. (2022). Efficacy of green cerium oxide nanoparticles for potential therapeutic applications: Circumstantial insight on mechanistic aspects. *Nanomaterials*, 12(12), 2117.
- Montini, T., Melchionna, M., Monai, M., & Fornasiero, P. (2016). Fundamentals and catalytic applications of CeO<sub>2</sub>-based materials. *Chemical reviews*, 116(10), 5987-6041.
- Garzon, F. H., Mukundan, R., & Brosha, E. L. (2000). Solid-state mixed potential gas sensors: theory, experiments and challenges. *Solid State Ionics*, 136, 633-638.
- Vigneselvan, S., Manikandan, V., Petrila, I., Vanitha, A., & Chandrasekaran, J. (2020). Effect of copper substitution on structural, optical and humidity-sensing characteristics of cerium oxide nanoparticles. *Journal of Physics and Chemistry of Solids*, 136, 109173.
- Thakur, S., & Patil, P. (2014). Rapid synthesis of cerium oxide nanoparticles with superior humidity-sensing performance. *Sensors and Actuators B: Chemical*, 194, 260-268.
- Mazur, F., Han, Z., Tjandra, A. D., & Chandrawati, R. (2024). Digitalization of colorimetric sensor technologies for food safety. *Advanced Materials*, 36(42), 2404274.
- Subbiah, D. K., Kulandaisamy, A. J., George, R. B., Shankar, P., Mani, G. K., Babu, K. J., & Rayappan, J. B. B. (2018). Nano ceria as xylene sensor–Role of cerium precursor. *Journal of Alloys and Compounds*, 753, 771-780.
- Qian, J., Wang, Y., Pan, J., Chen, Z., Wang, C., Chen, J., & Wu, Z. (2020). Non-enzymatic glucose sensor based on ZnO–CeO<sub>2</sub> whiskers. *Materials Chemistry and Physics*, 239, 122051.
- Kim, N. W., Lee, D. K., & Yu, H. (2019). Selective shape control of cerium oxide nanocrystals for photocatalytic and chemical sensing effect. *RSC advances*, 9(24), 13829-13837.
- Liao, L., Mai, H. X., Yuan, Q., Lu, H. B., Li, J. C., Liu, C., ... & Yu, T. (2008). Single CeO<sub>2</sub> nanowire gas sensor supported with Pt nanocrystals: gas



sensitivity, surface bond states, and chemical mechanism. *The Journal of Physical Chemistry C*, 112(24), 9061-9065.

- Allasi, H. L., Rajalingam, A. A., Jani, S. P., & Uppalapati, S. (2023). Influence of synthesized (green) cerium oxide nanoparticle with neem (*Azadirachta indica*) oil biofuel. *Bulletin of the Chemical Society of Ethiopia*, 37(2), 477-490.
- González-Mancebo, D., Becerro, A. I., Rojas, T. C., Olivencia, A., Corral, A., Balcerzyk, M., ... & Ocaña, M. (2018). Room temperature synthesis of water-dispersible Ln<sup>3+</sup>: CeF<sub>3</sub> (Ln= Nd, Tb) nanoparticles with different morphology as bimodal probes for fluorescence and CT imaging. *Journal of Colloid and Interface Science*, 520, 134-144.
- Arunachalam, T., Karpagasundaram, M., & Rajarathinam, N. (2017). Ultrasound assisted green synthesis of cerium oxide nanoparticles using *Prosopis juliflora* leaf extract and their structural, optical and antibacterial properties. *Materials Science-Poland*, 35(4), 791-798.
- Muthuvel, A., Jothibas, M., Manoharan, C., & Jayakumar, S. J. (2020). Synthesis of CeO<sub>2</sub> NPs by chemical and biological methods and their photocatalytic, antibacterial and in vitro antioxidant activity. *Research on Chemical Intermediates*, 46, 2705-2729
- Bartůňek, V., Rak, J., Král, V., & Smrčková, O. (2011). Simple one-step preparation of cerium trifluoride nanoparticles. *Journal of Fluorine Chemistry*, 132(4), 298-301.
- Sun, C., Li, H., Zhang, H., Wang, Z., & Chen, L. (2005). Controlled synthesis of CeO<sub>2</sub> nanorods by a solvothermal method. *Nanotechnology*, 16(9), 1454.
- Hewer, T. L., Soeira, L. S., Brito, G. E., & Freire, R. S. (2013). One-pot green synthesis of cerium oxide-carbon microspheres and their catalytic ozonation activity. *Journal of Materials Chemistry A*, 1(20), 6169-6174 .
- Bear, J. C., McNaughten, P. D., Southern, P., O'Brien, P., & Dunnill, C. W. (2015). Nickel-doped ceria nanoparticles: the effect of annealing on room temperature ferromagnetism. *Crystals*, 5(3), 312-326.
- Ivanov, V. K., Shcherbakov, A. B., & Usatenko, A. V. (2009). Structure-sensitive properties and biomedical applications of nanodispersed cerium dioxide. *Russian chemical reviews*, 78(9), 855.
- An, K., Long, C., Sui, Y., Qing, Y., Zhao, G., An, Z., ... & Liu, C. (2020). Large-scale preparation of superhydrophobic cerium dioxide nanocomposite coating with UV resistance, mechanical robustness, and anti-corrosion properties. *Surface and Coatings Technology*, 384, 125312.
- Fu, Y. P., Wen, S. B., & Lu, C. H. (2008). Preparation and characterization of samaria-doped ceria electrolyte materials for solid oxide fuel cells. *Journal of the American Ceramic Society*, 91(1), 127-131.

- Ecco, L. G., Rossi, S., Deflorian, F., & Fedel, M. (2018). Colloidal cerium oxide nanoparticles: preparation and corrosion inhibition performance on AA5005 aluminum alloy. *Journal of The Electrochemical Society*, 165(2), C86.
  - Elahi, B., Mirzaee, M., Darroudi, M., Oskuee, R. K., Sadri, K., & Amiri, M. S. (2019). Preparation of cerium oxide nanoparticles in *Salvia MacrosiphonBoiss* seeds extract and investigation of their photo-catalytic activities. *Ceramics International*, 45(4), 4790-4797.
  - Cao, W., Ju, P., Wang, Z., Zhang, Y., Zhai, X., Jiang, F., & Sun, C. (2020). Colorimetric detection of H<sub>2</sub>O<sub>2</sub> based on the enhanced peroxidase mimetic activity of nanoparticles decorated Ce<sub>2</sub> (WO<sub>4</sub>)<sub>3</sub> nanosheets. *Spectrochimica Acta Part A: Molecular and Biomolecular Spectroscopy*, 239, 118499.
  - Kumar, S., Ojha, A. K., Patrice, D., Yadav, B. S., & Materny, A. (2016). One-step in situ synthesis of CeO<sub>2</sub> nanoparticles grown on reduced graphene oxide as an excellent fluorescent and photocatalyst material under sunlight irradiation. *Physical Chemistry Chemical Physics*, 18(16), 11157-11167.
  - Cuahtecontzi-Delint, R., Mendez-Rojas, M. A., Bandala, E. R., Quiroz, M. A., Recillas, S., & Sanchez-Salas, J. L. (2013). Enhanced antibacterial activity of CeO<sub>2</sub> nanoparticles by surfactants. *International Journal of Chemical Reactor Engineering*, 11(2), 781-785.
  - Lin, K. S., & Chowdhury, S. (2010). Synthesis, characterization, and application of 1-D cerium oxide nanomaterials: a review. *International journal of molecular sciences*, 11(9), 3226-3251.
  - Dos Santos, M. L., Lima, R. C., Riccardi, C. S., Tranquilin, R. L., Bueno, P. R., Varela, J. A., & Longo, E. (2008). Preparation and characterization of ceria nanospheres by microwave-hydrothermal method. *Materials Letters*, 62(30), 4509-4511.
  - Gao, F., Lu, Q., & Komarneni, S. (2006). Fast synthesis of cerium oxide nanoparticles and nanorods. *Journal of nanoscience and nanotechnology*, 6(12), 3812-3819.
  - Ji, Z., Wang, X., Zhang, H., Lin, S., Meng, H., Sun, B., ... & Zink, J. I. (2012). Designed synthesis of CeO<sub>2</sub> nanorods and nanowires for studying toxicological effects of high aspect ratio nanomaterials. *ACS nano*, 6(6), 5366-5380.
  - Bugayeva, N., & Robinson, J. (2007). Synthesis of hydrated CeO<sub>2</sub> nanowires and nanoneedles. *Materials science and technology*, 23(2), 237-241.
  - Zarinkamar, M., Farahmandjou, M., & Firoozabadi, T. P. (2016). One-step synthesis of ceria (CeO<sub>2</sub>) nano-spheres by a simple wet chemical method. *Journal of Ceramic Processing Research*, 17(3), 166-169.
- www.researchgate.net

- Hirano, M., & Kato, E. (1999). Hydrothermal synthesis of nanocrystalline cerium (IV) oxide powders. *Journal of the American Ceramic Society*, 82(3), 786-788.
- Zhang, Y., Kang, Z., Dong, J., Abernathy, H., & Liu, M. (2006). Self-assembly of cerium compound nanopetals via a hydrothermal process: Synthesis, formation mechanism and properties. *Journal of Solid State Chemistry*, 179(6), 1733-1738.
- Masui, T., Hirai, H., Imanaka, N., Adachi, G., Sakata, T., & Mori, H. (2002). Synthesis of cerium oxide nanoparticles by hydrothermal crystallization with citric acid. *Journal of Materials Science Letters*, 21, 489-491.
- Chen, H. I., & Chang, H. Y. (2004). Homogeneous precipitation of cerium dioxide nanoparticles in alcohol/water mixed solvents. *Colloids and Surfaces A: Physicochemical and Engineering Aspects*, 242(1-3), 61-69.
- Chen, H. I., & Chang, H. Y. (2005). Synthesis of nanocrystalline cerium oxide particles by the precipitation method. *Ceramics International*, 31(6), 795-802.
- Yin, L., Wang, Y., Pang, G., Koltypin, Y., & Gedanken, A. (2002). Sonochemical synthesis of cerium oxide nanoparticles—effect of additives and quantum size effect. *Journal of Colloid and Interface Science*, 246(1), 78-84.
- Pinjari, D. V., & Pandit, A. B. (2011). Room temperature synthesis of crystalline CeO<sub>2</sub> nanopowder: advantage of sonochemical method over conventional method. *Ultrasonics sonochemistry*, 18(5), 1118-1123.
- Li, Y. X., Chen, W. F., Zhou, X. Z., Gu, Z. Y., & Chen, C. M. (2005). Synthesis of CeO<sub>2</sub> nanoparticles by mechanochemical processing and the inhibiting action of NaCl on particle agglomeration. *Materials Letters*, 59(1), 48-52.
- Hu, C., Zhang, Z., Liu, H., Gao, P., & Wang, Z. L. (2006). Direct synthesis and structure characterization of ultrafine CeO<sub>2</sub> nanoparticles. *Nanotechnology*, 17(24), 5983.
- Gu, H., & Soucek, M. D. (2007). Preparation and characterization of monodisperse cerium oxide nanoparticles in hydrocarbon solvents. *Chemistry of Materials*, 19(5), 1103-1110.
- Bumajdad, A., Eastoe, J., & Mathew, A. (2009). Cerium oxide nanoparticles prepared in self-assembled systems. *Advances in colloid and interface science*, 147, 56-66.
- Zeljković, S., Jelić, D., Maruyama, H., & Nino, J. C. (2019). Solvent-deficient synthesis of cerium oxide: Characterization and kinetics. *Ceramics International*, 45(8), 10063-10071.
- Chelliah, M., Rayappan, J. B. B., & Krishnan, U. M. (2012). Synthesis and characterization of cerium oxide nanoparticles by hydroxide mediated approach. *Journal of Applied Sciences*, 12(16), 1734-1737..

- Lakhota, S. R., Mukhopadhyay, M., & Kumari, P. (2018). Cerium oxide nanoparticles embedded thin-film nanocomposite nanofiltration membrane for water treatment. *Scientific reports*, 8(1), 4976.
- Huang, P. X., Wu, F., Zhu, B. L., Gao, X. P., Zhu, H. Y., Yan, T. Y., ... & Song, D. Y. (2005). CeO<sub>2</sub> nanorods and gold nanocrystals supported on CeO<sub>2</sub> nanorods as catalyst. *The Journal of Physical Chemistry B*, 109(41), 19169-19174.
- Swetha, B., Julian, O., Shashank, S., Nicholas, E., Rameech, M., Soumen, D., ... & Sudipta, S. (2017). Modulating the Catalytic Activity of Cerium Oxide Nanoparticles with the Anion of the Precursor Salt. *pubs.acs.org* on August 22, 2017.
- Wang, W., Howe, J. Y., Li, Y., Qiu, X., Joy, D. C., Paranthaman, M. P., ... & Gu, B. (2010). A surfactant and template-free route for synthesizing ceria nanocrystals with tunable morphologies. *Journal of Materials Chemistry*, 20(36), 7776-7781.
- Reshma, P., & Ashwini, K. (2017). Cerium Oxide Nanoparticles: Synthesis, Characterization and Study of Antimicrobial Activity. *J Nanomater Mol Nanotechnol* 6: 3. of, 4, 1-4.
- Cui, R., Lu, W., Zhang, L., Yue, B., & Shen, S. (2009). Template-free synthesis and self-assembly of CeO<sub>2</sub> nanospheres fabricated with foursquare nanoflakes. *The Journal of Physical Chemistry C*, 113(52), 21520-21525.
- Abbas, F., Iqbal, J., Jan, T., Badshah, N., Mansoor, Q., & Ismail, M. (2016). Structural, morphological, Raman, optical, magnetic, and antibacterial characteristics of CeO<sub>2</sub> nanostructures. *International Journal of Minerals, Metallurgy, and Materials*, 23, 102-108.
- Sehar, S., Naz, I., Rehman, A., Sun, W., Alhewairini, S. S., Zahid, M. N., & Younis, A. (2021). Shape-controlled synthesis of cerium oxide nanoparticles for efficient dye photodegradation and antibacterial activities. *Applied Organometallic Chemistry*, 35(1), e6069.
- Ghahramani, Z., Arabi, A. M., Shafiee Afarani, M., & Mahdavian, M. (2020). Solution combustion synthesis of cerium oxide nanoparticles as corrosion inhibitor. *International Journal of Applied Ceramic Technology*, 17(3), 1514-1521.
- Divya, T., Anjali, C., Sunajadevi, K. R., Anas, K., & Renuka, N. K. (2021). Influence of hydrothermal synthesis conditions on lattice defects in cerium oxide. *Journal of Solid State Chemistry*, 300, 122253.
- Mazhar, M. E., Bakhtawar, S., Rana, A. M., Usmani, M. N., Akhtar, N., Abbas, W., ... & Ahmad, J. (2019). Insight into the structural characterization of pure and Zr-doped hydrothermally synthesized cerium oxide nanoparticles. *Materials Research Express*, 6(10), 105022.

- Dos Santos, A. P. B., Dantas, T. C. M., Costa, J. A. P., Souza, L. D., Soares, J. M., Caldeira, V. P. S., ... & Santos, A. G. D. (2020). Formation of CeO<sub>2</sub> nanotubes through different conditions of hydrothermal synthesis. *Surfaces and Interfaces*, 21, 100746.
- Khadar, Y. S., Balamurugan, A., Devarajan, V. P., & Subramanian, R. (2017). Hydrothermal synthesis of gadolinium (Gd) doped cerium oxide (CeO<sub>2</sub>) nanoparticles: characterization and antibacterial activity. *Oriental Journal of Chemistry*, 33(5), 2405.
- Dhannia, T., Jayalekshmi, S., Kumar, M. S., Rao, T. P., & Bose, A. C. (2009). Effect of aluminium doping and annealing on structural and optical properties of cerium oxide nanocrystals. *Journal of Physics and Chemistry of Solids*, 70(11), 1443-1447.
- Dhannia, T., Jayalekshmi, S., Kumar, M. S., Rao, T. P., & Bose, A. C. (2010). Effect of iron doping and annealing on structural and optical properties of cerium oxide nanocrystals. *Journal of Physics and Chemistry of Solids*, 71(7), 1020-1025.
- Farahmandjou, M., & Dastpak, M. (2018). Fe-Loaded CeO<sub>2</sub> nanosized prepared by simple Co-precipitation route. *Physical Chemistry Research*, 6(4), 713-720.
- Renuka, N. K. (2012). Structural characteristics of quantum-size ceria nano particles synthesized via simple ammonia precipitation. *Journal of Alloys and Compounds*, 513, 230-235.
- Pathak, V., Lad, P., Thakkar, A. B., Thakor, P., Deshpande, M. P., & Pandya, S. (2023). Synthesis, characterization and applications of cubic fluorite cerium oxide nanoparticles: a comprehensive study. *Results in Surfaces and Interfaces*, 11, 100111.
- Aseena, S., Abraham, N., & Babu, V. S. (2023). Morphological and optical studies of zinc doped cerium oxide nanoparticles prepared by single step co-precipitation method. *Materials Today: Proceedings*, 80, 1901-1905.
- Ramachandran, M., Subadevi, R., & Sivakumar, M. (2019). Role of pH on synthesis and characterization of cerium oxide (CeO<sub>2</sub>) nano particles by modified co-precipitation method. *Vacuum*, 161, 220-224.
- Channei, D., Nakaruk, A., Jannoey, P., & Phanichphant, S. (2019). Preparation and characterization of Pd modified CeO<sub>2</sub> nanoparticles for photocatalytic degradation of dye. *Solid State Sciences*, 87, 9-14.
- Soren, S., Besso, M., & Parhi, P. (2015). A rapid microwave initiated polyol synthesis of cerium oxide nanoparticle using different cerium precursors. *Ceramics International*, 41(6), 8114-8118.
- Kumar, E., Selvarajan, P., & Muthuraj, D. (2013). Synthesis and characterization of CeO<sub>2</sub> nanocrystals by solvothermal route. *Materials Research*, 16, 269-276.

- Parvathy, S., & Venkatraman, B. R. (2017). Synthesis and characterization of various metal ions doped CeO<sub>2</sub> nanoparticles derived from the *Azadirachta indica* leaf extracts. *Chemical Science Transactions*, 6(4), 513-522.
- Gopinath, K., Karthika, V., Sundaravadivelan, C., Gowri, S., & Arumugam, A. (2015). Mycogenesis of cerium oxide nanoparticles using *Aspergillus niger* culture filtrate and their applications for antibacterial and larvicidal activities. *Journal of Nanostructure in Chemistry*, 5, 295-303.
- Sabouri, Z., Sabouri, M., Amiri, M. S., Khatami, M., & Darroudi, M. (2022). Plant-based synthesis of cerium oxide nanoparticles using *Rheum turkestanicum* extract and evaluation of their cytotoxicity and photocatalytic properties. *Materials Technology*, 37(8), 555-568.
- Kalaycıoğlu, Z., Geçim, B., & Erim, F. B. (2022). Green synthesis of cerium oxide nanoparticles from turmeric and kinds of honey: characterisations, antioxidant and photocatalytic dye degradation activities. *Advances in Natural Sciences: Nanoscience and Nanotechnology*, 13(1), 015016.
- Das, S., Panicker, N. J., Rather, M. A., Mandal, M., & Sahu, P. P. (2022). Green synthesis of cerium oxide nanoparticles using *Dillenia indica* aqueous extract and its anti-oxidant activity. *Bulletin of Materials Science*, 46(1), 3.
- Muthuvel, A., Jothibas, M., Mohana, V., & Manoharan, C. J. I. C. C. (2020). Green synthesis of cerium oxide nanoparticles using *Calotropis procera* flower extract and their photocatalytic degradation and antibacterial activity. *Inorganic Chemistry Communications*, 119, 108086.
- Kaygusuz, H., & Erim, F. B. (2020). Biopolymer-assisted green synthesis of functional cerium oxide nanoparticles. *Chemical Papers*, 74(7), 2357-2363.
- Irshad, M. S., Aziz, M. H., Fatima, M., Rehman, S. U., Idrees, M., Rana, S., ... & Huang, Q. (2019). Green synthesis, cytotoxicity, antioxidant and photocatalytic activity of CeO<sub>2</sub> nanoparticles mediated via orange peel extract (OPE). *Materials Research Express*, 6(9), 0950a4.
- Gunasekaran, N. K., Tumkur, P. P., Bayon, N. N., Prabhakaran, K., Arasho, W. D., Hall, J. C., & Ramesh, G. T. (2023). Cerium Oxide Nanoparticles: Synthesis and Characterization Using *Curcuma longa* (Turmeric Rhizome). *Energy and Environment Focus*, 7(1), 83-89.
- Druzian, D. M., Oviedo, L. R., Loureiro, S. N., Wouters, R. D., Vizzotto, B. S., de Oliveira Pinto, E., ... & da Silva, W. L. (2023). Cerium oxide nanoparticles: Biosynthesis, characterization, antimicrobial, ecotoxicity and photocatalytic activity. *Journal of Photochemistry and Photobiology A: Chemistry*, 442, 114773.
- Miri, A., Beiki, H., Najafidoust, A., Khatami, M., & Sarani, M. (2021). Cerium oxide nanoparticles: green synthesis using Banana peel, cytotoxic effect,



UV protection and their photocatalytic activity. *Bioprocess and Biosystems Engineering*, 44(9), 1891-1899.

- Elahi, B., Mirzaee, M., Darroudi, M., Oskuee, R. K., Sadri, K., & Gholami, L. (2020). Role of oxygen vacancies on photo-catalytic activities of green synthesized ceria nanoparticles in *Cydonia oblonga* miller seeds extract and evaluation of its cytotoxicity effects. *Journal of Alloys and Compounds*, 816, 152553.
- Sayed, M. A., Abo-Aly, M. M., Aziz, A. A. A., Hassan, A., & Salem, A. N. M. (2021). A facile hydrothermal synthesis of novel CeO<sub>2</sub>/CdSe and CeO<sub>2</sub>/CdTe Nanocomposites: Spectroscopic investigations for economically feasible photocatalytic degradation of Congo red dye. *Inorganic Chemistry Communications*, 130, 108750.
- Thomas, E., Briancon, S., Chaput, F., Magnano, G. C., Trenque, I., Arquier, D., ... & Bolzinger, M. A. (2024). Tailor-Made Synthesis of Cerium Oxide Nanoparticles for Improving the Skin Decontamination of Paraoxon. *ACS Applied Nano Materials*, 7(14), 16052-16065.
- Kusuma, K. B., Manju, M., Ravikumar, C. R., Raghavendra, N., Amulya, M. S., Nagaswarupa, H. P., ... & Shekhar, T. S. (2022). Photocatalytic degradation of Methylene Blue and electrochemical sensing of paracetamol using Cerium oxide nanoparticles synthesized via sonochemical route. *Applied Surface Science Advances*, 11, 100304.
- Jain, B., Singh, A. K., Hashmi, A., Susan, M. A. B. H., & Lellouche, J. P. (2020). Surfactant-assisted cerium oxide and its catalytic activity towards Fenton process for non-degradable dye. *Advanced Composites and Hybrid Materials*, 3, 430-441.
- Muthuvel, A., Jothibas, M., Mohana, V., & Manoharan, C. J. I. C. C. (2020). Green synthesis of cerium oxide nanoparticles using *Calotropis procera* flower extract and their photocatalytic degradation and antibacterial activity. *Inorganic Chemistry Communications*, 119, 108086.
- Feng KeJun, F. K., Song Biao, S. B., Li XianFeng, L. X., Liao FangLi, L. F., & Gong JiLai, G. J. (2019). Enhanced photocatalytic performance of magnetic multi-walled carbon nanotubes/cerium dioxide nanocomposite.
- Xu, T., Lei, X., Gu, G., Zou, R., & Wu, Q. (2019). Facile synthesis of CeO<sub>2</sub>-graphene oxide composites with enhanced visible-light photocatalytic performance. *Materials Science and Engineering: B*, 244, 49-55.
- Negi, K., Umar, A., Chauhan, M. S., & Akhtar, M. S. (2019). Ag/CeO<sub>2</sub> nanostructured materials for enhanced photocatalytic and antibacterial applications. *Ceramics International*, 45(16), 20509-20517.
- Zeleke, M. A., & Kuo, D. H. (2019). Synthesis and application of V<sub>2</sub>O<sub>5</sub>-CeO<sub>2</sub> nanocomposite catalyst for enhanced degradation of methylene blue under visible light illumination. *Chemosphere*, 235, 935-944.

- Li, H., Wang, G., Zhang, F., Cai, Y., Wang, Y., & Djerdj, I. (2012). Surfactant-assisted synthesis of CeO<sub>2</sub> nanoparticles and their application in wastewater treatment. *Rsc Advances*, 2(32), 12413-12423.
- Mishra, S., Soren, S., Debnath, A. K., Aswal, D. K., Das, N., & Parhi, P. (2018). Rapid microwave-Hydrothermal synthesis of CeO<sub>2</sub> nanoparticles for simultaneous adsorption/photodegradation of organic dyes under visible light. *Optik*, 169, 125-136.
- Raees, A., Jamal, M. A., Ahmed, I., Silanpaa, M., & Saad Algarni, T. (2021). Synthesis and characterization of CeO<sub>2</sub>/CuO nanocomposites for photocatalytic degradation of methylene blue in visible light. *Coatings*, 11(3), 305.
- Krishnan, A., Vishwanathan, P. V., Mohan, A. C., Panchami, R., Viswanath, S., & Krishnan, A. V. (2021). Tuning of photocatalytic performance of CeO<sub>2</sub>-Fe<sub>2</sub>O<sub>3</sub> composite by Sn-doping for the effective degradation of methylene blue (MB) and methyl orange (MO) dyes. *Surfaces and Interfaces*, 22, 100808.
- Magdalane, C. M., Kaviyarasu, K., Vijaya, J. J., Siddhardha, B., & Jeyaraj, B. (2017). Facile synthesis of heterostructured cerium oxide/yttrium oxide nanocomposite in UV light induced photocatalytic degradation and catalytic reduction: synergistic effect of antimicrobial studies. *Journal of Photochemistry and Photobiology B: Biology*, 173, 23-34.
- Arul, N. S., Mangalaraj, D., Chen, P. C., Ponpandian, N., Meena, P., & Masuda, Y. (2012). Enhanced photocatalytic activity of cobalt-doped CeO<sub>2</sub> nanorods. *Journal of sol-gel science and technology*, 64, 515-523.
- Saranya, J., Ranjith, K. S., Saravanan, P., Mangalaraj, D., & Kumar, R. T. R. (2014). Cobalt-doped cerium oxide nanoparticles: enhanced photocatalytic activity under UV and visible light irradiation. *Materials science in semiconductor processing*, 26, 218-224.
- Ahmad, T., Iqbal, J., Bustam, M. A., Zulfiqar, M., Muhammad, N., Al Hajeri, B. M., ... & Ullah, S. (2020). Phytosynthesis of cerium oxide nanoparticles and investigation of their photocatalytic potential for degradation of phenol under visible light. *Journal of Molecular Structure*, 1217, 128292.
- Iqbal, J., Shah, N. S., Sayed, M., Muhammad, N., Khan, J. A., Khan, Z. U. H., ... & Polychronopoulou, K. (2020). Deep eutectic solvent-mediated synthesis of ceria nanoparticles with the enhanced yield for photocatalytic degradation of flumequine under UV-C. *Journal of Water Process Engineering*, 33, 101012.
- Zheng, X., Huang, S., Yang, D., Zhai, H., You, Y., Fu, X., ... & Liu, Y. (2017). Synthesis of X-architecture CeO<sub>2</sub> for the photodegradation of methylene blue under UV-light irradiation. *Journal of Alloys and Compounds*, 705, 131-137.

- El Rouby, W. M. A., Farghali, A. A., &Hamdedein, A. (2016). Microwave synthesis of pure and doped cerium (IV) oxide (CeO<sub>2</sub>) nanoparticles for methylene blue degradation. *Water Science and Technology*, 74(10), 2325-2336.
- Ravishankar, T. N., Ramakrishnappa, T., Nagaraju, G., & Rajanaika, H. (2015). Synthesis and characterization of CeO<sub>2</sub> nanoparticles via solution combustion method for photocatalytic and antibacterial activity studies. *ChemistryOpen*, 4(2), 146-154.
- Afza, N., Shivakumar, M. S., Alam, M. W., Kumar, A. N., Bhatt, A. S., Murthy, H. A., ... &Selvanandan, S. (2022). Facile hydrothermal synthesis of cerium oxide/rGO nanocomposite for photocatalytic and supercapacitor applications. *Applied Surface Science Advances*, 11, 100307.
- Ahmad, T., Iqbal, J., Bustam, M. A., Zulfiqar, M., Muhammad, N., Al Hajeri, B. M., ... & Ullah, S. (2020). Phytosynthesis of cerium oxide nanoparticles and investigation of their photocatalytic potential for degradation of phenol under visible light. *Journal of Molecular Structure*, 1217, 128292.
- Safat, S., Buazar, F., Albukhaty, S., &Matroodi, S. (2021). Enhanced sunlight photocatalytic activity and biosafety of marine-driven synthesized cerium oxide nanoparticles. *Scientific Reports*, 11(1), 14734.
- Surendra, T. V., & Roopan, S. M. (2016). Photocatalytic and antibacterial properties of phytosynthesized CeO<sub>2</sub> NPs using *Moringa oleifera* peel extract. *Journal of Photochemistry and Photobiology B: Biology*, 161, 122-128.
- Magudieshwaran, R., Ishii, J., Raja, K. C. N., Terashima, C., Venkatachalam, R., Fujishima, A., &Pitchaimuthu, S. (2019). Green and chemical synthesized CeO<sub>2</sub> nanoparticles for photocatalytic indoor air pollutant degradation. *Materials Letters*, 239, 40-44.
- Sharma, J. K., Srivastava, P., Ameen, S., Akhtar, M. S., Sengupta, S. K., & Singh, G. (2017). Phytoconstituents assisted green synthesis of cerium oxide nanoparticles for thermal decomposition and dye remediation. *Materials Research Bulletin*, 91, 98-107.
- Gnanam, S., Gajendiran, J., Ramya, J. R., Ramachandran, K., & Raj, S. G. (2021). Glycine-assisted hydrothermal synthesis of pure and europium doped CeO<sub>2</sub> nanoparticles and their structural, optical, photoluminescence, photocatalytic and antibacterial properties. *Chemical Physics Letters*, 763, 138217.
- Magdalane, C. M., Kaviyarasu, K., Raja, A., Arularasu, M. V., Mola, G. T., Isaev, A. B., ... &Maaza, M. (2018). Photocatalytic decomposition effect of erbium doped cerium oxide nanostructures driven by visible light irradiation: investigation of cytotoxicity, antibacterial growth inhibition using catalyst. *Journal of Photochemistry and Photobiology B: Biology*, 185, 275-282.

- Jayakumar, G., Irudayaraj, A. A., & Raj, A. D. (2017). Particle size effect on the properties of cerium oxide (CeO<sub>2</sub>) nanoparticles synthesized by hydrothermal method. *Mechanics, Materials Science & Engineering Journal*, 9(1).
- Kim, N. W., Lee, D. K., & Yu, H. (2019). Selective shape control of cerium oxide nanocrystals for photocatalytic and chemical sensing effect. *RSC advances*, 9(24), 13829-13837.
- Reddy Yadav, L. S., Manjunath, K., Archana, B., Madhu, C., Raja Naika, H., Nagabhushana, H., ... & Nagaraju, G. (2016). Fruit juice extract mediated synthesis of CeO<sub>2</sub> nanoparticles for antibacterial and photocatalytic activities. *The European Physical Journal Plus*, 131, 1-10.
- Zhang, M., Zhang, C., Zhai, X., Luo, F., Du, Y., & Yan, C. (2019). Antibacterial mechanism and activity of cerium oxide nanoparticles. *Sci. China Mater*, 62(11), 1727-1739.
- LU, X. W., QIAN, J. C., Feng, C. H. E. N., LI, X. Z., & CHEN, Z. G. (2012). Synthesis, characterization and antibacterial property of Ag/mesoporous CeO<sub>2</sub> nanocomposite material. *Transactions of Nonferrous Metals Society of China*, 22(6), 1418-1422.
- Yue, L., & Zhang, X. M. (2009). Structural characterization and photocatalytic behaviors of doped CeO<sub>2</sub> nanoparticles. *Journal of Alloys and Compounds*, 475(1-2), 702-705.
- Maleki, P., Nemati, F., Gholoobi, A., Hashemzadeh, A., Sabouri, Z., & Darroudi, M. (2021). Green facile synthesis of silver-doped cerium oxide nanoparticles and investigation of their cytotoxicity and antibacterial activity. *Inorganic Chemistry Communications*, 131, 108762.
- Balamurugan, A., Sudha, M., Surendhiran, S., Anandarasu, R., Ravikumar, S., & Khadar, Y. S. (2020). Hydrothermal synthesis of samarium (Sm) doped cerium oxide (CeO<sub>2</sub>) nanoparticles: characterization and antibacterial activity. *Materials Today: Proceedings*, 26, 3588-3594.
- Kannan, S. K., & Sundrarajan, M. (2014). A green approach for the synthesis of a cerium oxide nanoparticle: characterization and antibacterial activity. *International journal of nanoscience*, 13(03), 1450018.
- Pelletier, D. A., Suresh, A. K., Holton, G. A., McKeown, C. K., Wang, W., Gu, B., ... & Doktycz, M. J. (2010). Effects of engineered cerium oxide nanoparticles on bacterial growth and viability. *Applied and environmental microbiology*, 76(24), 7981-7989.
- Kareem, M. T., & Hamdan, S. A. (2024, February). Study of the influence concentration difference in properties of cerium thin films. In *AIP Conference Proceedings* (Vol. 2922, No. 1). AIP Publishing.
- Altaf, M., Manoharadas, S., & Zeyad, M. T. (2021). Green synthesis of cerium oxide nanoparticles using *Acorus calamus* extract and their

antibiofilm activity against bacterial pathogens. *Microscopy Research and Technique*, 84(8), 1638-1648.

- Sathiyapriya, R., Balaji, M., & Rajesh, S. (2020). Bio-synthesis of cerium oxide nanoparticles from *Coriandrum sativum* L. leaf extract and their antibacterial activity. *International Journal of Advanced Science, Engineering*, 6, 1439-1444.
- Magdalane, C. M., Kaviyarasu, K., Vijaya, J. J., Siddhardha, B., & Jeyaraj, B. (2016). Photocatalytic activity of binary metal oxide nanocomposites of CeO<sub>2</sub>/CdO nanospheres: investigation of optical and antimicrobial activity. *Journal of Photochemistry and Photobiology B: Biology*, 163, 77-86.
- Devi, N. S., Ganapathy, D. M., Rajeshkumar, S., & Maiti, S. (2022). Characterization and antimicrobial activity of cerium oxide nanoparticles synthesized using neem and ginger. *Journal of Advanced Pharmaceutical Technology & Research*, 13(Suppl 2), S491-S495.
- Ahmed, H. E., Iqbal, Y., Aziz, M. H., Atif, M., Batool, Z., Hanif, A., ... & Ahmad, H. (2021). Green synthesis of CeO<sub>2</sub> nanoparticles from the *Abelmoschus esculentus* extract: evaluation of antioxidant, anticancer, antibacterial, and wound-healing activities. *Molecules*, 26(15), 4659.
- Rahdar, A., Beyzaei, H., Askari, F., & Kyzas, G. Z. (2020). Gum-based cerium oxide nanoparticles for antimicrobial assay. *Applied Physics A*, 126, 1-9.
- Park, E. J., Choi, J., Park, Y. K., & Park, K. (2008). Oxidative stress induced by cerium oxide nanoparticles in cultured BEAS-2B cells. *Toxicology*, 245(1-2), 90-100.
- Renu, G., Rani, V. V., Nair, S. V., Subramanian, K. R. V., & Lakshmanan, V. K. (2012). Development of cerium oxide nanoparticles and its cytotoxicity in prostate cancer cells. *Advanced Science Letters*, 6(1), 17-25.
- Darroudi, M., Hakimi, M., Sarani, M., Oskuee, R. K., Zak, A. K., & Gholami, L. (2013). Facile synthesis, characterization, and evaluation of neurotoxicity effect of cerium oxide nanoparticles. *Ceramics International*, 39(6), 6917-6921.
- Bazhukova, I. N., Sokovnin, S. Y., Ilves, V. G., Myshkina, A. V., Vazirov, R. A., Pizurova, N., & Kasyanova, V. V. (2019). Luminescence and optical properties of cerium oxide nanoparticles. *Optical Materials*, 92, 136-142.
- Atif, M., Iqbal, S., Fakhar-e-Alam, M., Mansoor, Q., Alimgeer, K. S., Fatehmulla, A., ... & Chu, Y. M. (2021). Manganese-doped cerium oxide nanocomposite as a therapeutic agent for MCF-7 adenocarcinoma cell line. *Saudi Journal of Biological Sciences*, 28(2), 1233-1238.
- Abbas, F., Jan, T., Iqbal, J., Naqvi, M. S. H., & Ahmad, I. (2016). Inhibition of Neuroblastoma cancer cells viability by ferromagnetic Mn doped CeO<sub>2</sub> monodisperse nanoparticles mediated through reactive oxygen species. *Materials Chemistry and Physics*, 173, 146-151.

- Abbas, F., Iqbal, J., Maqbool, Q., Jan, T., Ullah, M. O., Nawaz, B., ... & Ahmad, I. (2017). ROS mediated malignancy cure performance of morphological, optical, and electrically tuned Sn doped CeO<sub>2</sub> nanostructures. *AIP Advances*, 7(9).
- Abbas, F., Jan, T., Iqbal, J., Ahmad, I., Naqvi, M. S. H., & Malik, M. (2015). Facile synthesis of ferromagnetic Ni doped CeO<sub>2</sub> nanoparticles with enhanced anticancer activity. *Applied Surface Science*, 357, 931-936.
- Lin, Y. H., Shen, L. J., Chou, T. H., & Shih, Y. H. (2021). Synthesis, stability, and cytotoxicity of novel cerium oxide nanoparticles for biomedical applications. *Journal of Cluster Science*, 32, 405-413.
- Miri, A., & Sarani, M. (2018). Biosynthesis, characterization and cytotoxic activity of CeO<sub>2</sub> nanoparticles. *Ceramics International*, 44(11), 12642-12647.
- Miri, A., Darroudi, M., & Sarani, M. (2020). Biosynthesis of cerium oxide nanoparticles and its cytotoxicity survey against colon cancer cell line. *Applied Organometallic Chemistry*, 34(1), e5308.
- Kargar, H., Ghazavi, H., & Darroudi, M. (2015). Size-controlled and bio-directed synthesis of ceria nanopowders and their in vitro cytotoxicity effects. *Ceramics International*, 41(3), 4123-4128.
- Zhong, L. S., Hu, J. S., Cao, A. M., Liu, Q., Song, W. G., & Wan, L. J. (2007). 3D flowerlike ceria micro/nanocomposite structure and its application for water treatment and CO removal. *Chemistry of Materials*, 19(7), 1648-1655.
- Nourmohammadi, E., Oskuee, R. K., Hasanzadeh, L., Mohajeri, M., Hashemzadeh, A., Rezayi, M., & Darroudi, M. (2018). Cytotoxic activity of greener synthesis of cerium oxide nanoparticles using carrageenan towards a WEHI 164 cancer cell line. *Ceramics International*, 44(16), 19570-19575.
- Ashna, M., Es-Haghi, A., Karimi Noghondar, M., Al Amara, D., & Yazdi, M. E. T. (2022). Greener synthesis of cerium oxide nanoemulsion using pollen grains of *Brassica napus* and evaluation of its antitumour and cytotoxicity properties. *Materials Technology*, 37(8), 525-532.
- Javadi, F., Yazdi, M. E. T., Baghani, M., & Es-haghi, A. (2019). Biosynthesis, characterization of cerium oxide nanoparticles using *Ceratonia siliqua* and evaluation of antioxidant and cytotoxicity activities. *Materials Research Express*, 6(6), 065408.
- Sridharan, M., Kamaraj, P., Arockiaselvi, J., Pushpamalini, T., Vivekanand, P. A., & Kumar, S. H. (2021). Synthesis, characterization and evaluation of biosynthesized Cerium oxide nanoparticle for its anticancer activity on breast cancer cell (MCF 7). *Materials Today: Proceedings*, 36, 914-919.
- Abbasi, N., Homayouni Tabrizi, M., Ardalan, T., & Roumi, S. (2022). Cerium oxide nanoparticles-loaded on chitosan for the investigation of anticancer properties. *Materials Technology*, 37(10), 1439-1449.



- Kermani, G., Karimi, E., & Tabrizi, M. H. (2022). Hybrid nanoarchitectonics of chitosan-cerium oxide nanoparticles for anticancer potentials. *Journal of Inorganic and Organometallic Polymers and Materials*, 32(7), 2591-2599.
- Schubert, D., Dargusch, R., Raitano, J., & Chan, S. W. (2006). Cerium and yttrium oxide nanoparticles are neuroprotective. *Biochemical and biophysical research communications*, 342(1), 86-91.
- Zholobak, N. M., Shcherbakov, A. B., Ivanova, O. S., Reukov, V., Baranchikov, A. E., & Ivanov, V. K. (2020). Nanoceria-curcumin conjugate: Synthesis and selective cytotoxicity against cancer cells under oxidative stress conditions. *Journal of Photochemistry and Photobiology B: Biology*, 209, 111921.
- Parvathya, S., & Venkatramanb, B. R. (2017). In vitro antibacterial and anticancer potential of CeO<sub>2</sub> nanoparticles prepared by co-precipitation and green synthesis method. *J. Nanosci. Curr. Res*, 2(02), 1-9.
- Ganeshkar, M. P., Goder, P. H., Mirjankar, M. R., Gaddigal, A. T., Shivappa, P., & Kamanavalli, C. M. (2024). Characterization and screening of anticancer properties of cerium oxide nanoparticles synthesized using *Averrhoa carambola* plant extract. *Inorganic and Nano-Metal Chemistry*, 54(8), 779-792.
- Nazaripour, E., Mousazadeh, F., Moghadam, M. D., Najafi, K., Borhani, F., Sarani, M., ... & Khatami, M. (2021). Biosynthesis of lead oxide and cerium oxide nanoparticles and their cytotoxic activities against colon cancer cell line. *Inorganic Chemistry Communications*, 131, 108800.
- Hamidian, K., Saberian, M. R., Miri, A., Sharifi, F., & Sarani, M. (2021). Doped and un-doped cerium oxide nanoparticles: Biosynthesis, characterization, and cytotoxic study. *Ceramics International*, 47(10), 13895-13902.
- Alghamdi, A. A. (2023). Biogenic Mg doped CeO<sub>2</sub> nanoparticles via *Hibiscus sabdariffa* and its potential biological applications. *Journal of Umm Al-Qura University for Applied Sciences*, 9(2), 132-141.
- Taherzadeh, D., Amiri, H., Ebrahimi, S., Ghafarpour, A., Samandarinejad, N., Darroudi, M., & Hashemy, S. I. (2023). Green synthesis of cerium oxide nanoparticles using *Falcaria Vulgaris* leaf extract and its anti-tumoral effects in prostate cancer.
- Nourmohammadi, E., Oskuee, R. K., Hasanzadeh, L., Mohajeri, M., Hashemzadeh, A., Rezayi, M., & Darroudi, M. (2018). Cytotoxic activity of greener synthesis of cerium oxide nanoparticles using carrageenan towards a WEHI 164 cancer cell line. *Ceramics International*, 44(16), 19570-19575.
- Soren, S., Jena, S. R., Samanta, L., & Parhi, P. (2015). Antioxidant potential and toxicity study of the cerium oxide nanoparticles synthesized by

microwave-mediated synthesis. *Applied biochemistry and biotechnology*, 177, 148-161.

- Hirst, S. M., Karakoti, A. S., Tyler, R. D., Sriranganathan, N., Seal, S., & Reilly, C. M. (2009). Anti-inflammatory properties of cerium oxide nanoparticles. *Small*, 5(24), 2848-2856.
- Patil, S. N., Paradeshi, J. S., Chaudhari, P. B., Mishra, S. J., & Chaudhari, B. L. (2016). Bio-therapeutic potential and cytotoxicity assessment of pectin-mediated synthesized nanostructured cerium oxide. *Applied Biochemistry and Biotechnology*, 180, 638-654.
- Shlapa, Y., Solopan, S., Sarnatskaya, V., Siposova, K., Gargarova, I., Veltruska, K., ... & Belous, A. (2022). Cerium dioxide nanoparticles synthesized via precipitation at constant pH: Synthesis, physical-chemical and antioxidant properties. *Colloids and Surfaces B: Biointerfaces*, 220, 112960.
- Chaudhary, R. G., Chouke, P. B., Bagade, R. D., Potbhare, A. K., & Dadure, K. M. (2020). Molecular docking and antioxidant activity of *Cleome simplicifolia* assisted synthesis of cerium oxide nanoparticles. *Materials Today: Proceedings*, 29, 1085-1090.
- Gallucci, N., Vitiello, G., Di Girolamo, R., Imbimbo, P., Monti, D. M., Tarallo, O., ... & Paduano, L. (2021). Towards the development of antioxidant cerium oxide nanoparticles for biomedical applications: Controlling the properties by tuning synthesis conditions. *Nanomaterials*, 11(2), 542.
- Singh, S., Kumar, U., Gittess, D., Sakthivel, T. S., Babu, B., & Seal, S. (2021). Cerium oxide nanomaterial with dual antioxidative scavenging potential: Synthesis and characterization. *Journal of Biomaterials Applications*, 36(5), 834-842.
- Dutta, D., Mukherjee, R., Ghosh, S., Patra, M., Mukherjee, M., & Basu, T. (2022). Cerium oxide nanoparticles as antioxidant or pro-oxidant agents. *ACS Applied Nano Materials*, 5(1), 1690-1701.